# AN ABSTRACT OF THE THESIS OF

Michael C. Frech for the degree of Master of Science in
Atmospheric Sciences presented on December 17, 1993.

Title:     A Nonlocal Mixing Formulation
for the Atmospheric Boundary Layer

Abstract approved:_____ Redacted for Privacy_

A two-scale approach for the turbulent mixing of momentum in an unstable stratified boundary layer is proposed in an attempt to eliminate existing inconsistencies between parameterized mixing of heat and momentum. The parameterization of the large eddy stress is suitable for simple boundary layer models where computational efficiency is important. We test the proposed formulation in a simple boundary layer model and compare predicted momentum profiles with Lidar mean momentum profiles from FIFE 1989. We examine the sensitivity of the proposed mixing scheme to baroclinicity. While the proposed two-scale approach is able to better predict observed conditions of well mixed momentum profiles, the complexity of momentum transport in baroclinic conditions is not well approximated.

A Nonlocal Mixing Formulation

for the Atmospheric Boundary Layer

by

Michael C. Frech

A THESIS

submitted to

Oregon State University

in partial fulfillment of the

requirements for the degree of

Master of Science

Completed December 17, 1993

Commencement June 1994.

APPROVED:

_____

Professor of Atmospheric Sciences in charge of major

_____

Dean of College of Oceanic and Atmospheric Sciences

_____

Dean of Graduate School

Date thesis presented _____ December 17, 1993 _____

Typed by Michael Frech for _____ Michael C. Frech _____

# ACKNOWLEDGEMENTS

# Table of Contents

# List of Figures

# List of Tables

# A Nonlocal Mixing Formulation
# for the Atmospheric Boundary Layer

# Chapter 1

# Introduction

In the heated boundary layer, eddies on the scale of the boundary layer dominate the vertical transport of heat and other quantities, especially in the middle and upper part of the boundary layer. These eddies normally assume the form of thermals or sheared-thermals and lead to transport by mixing in the presence of a bulk gradient across the boundary layer. The resulting heat flux may be counter to the local gradient in the middle and upper part of the boundary layer. For this reason Priestley and Swinbank (1947) modified the usual eddy diffusivity formulation to include a correction due to boundary layer scale transport. The eddy diffusivity represents local diffusion by small scale turbulence and cannot account for the transport by the larger scale eddies. This correction was formalized in terms of free convection similarity theory by Deardorff (1972). Troen and Mahrt (1986) generalized this formulation to include the effect of shear driven mixing and applied the formulation to moisture transport as well. Holtslag and Moeng (1991) also generalized this approach to accommodate bottom-up, top-down diffusion and to allow the nonlocal mixing coefficient to vanish smoothly with decreasing instability. Holtslag and Boville (1992) reformulated this smoothness condition in terms of readily available model variables. They explicitly show how the use of only an eddy diffusivity without a nonlocal correction leads to serious underestimation of the depth of mixing. We will refer to the above nonlocal approaches as two-scale mixing formulations consisting of small scale diffusion by an eddy diffusivity and large scale mixing by a nonlocal term or gradient correction. Two-scale mixing formulations are physically oversimplified, however, they seem to be enjoying increasing application because models with more complete physics require prohibitive resolution or lead to

poor results in one or more of the numerous meteorological situations encountered in global or operational models.

In Chapter 2, we show how two-scale mixing can be derived from a more general point of view. We then extend this approach to include mixing of momentum by large eddies. We will also identify certain inconsistencies with the existing two-scale approaches. Finally we will directly compare the above formulation with observed atmospheric flux data and improved wind profile information which has been previously lacking.

The previous two-scale formulations have not included the influence of transport of momentum by boundary-layer scale eddies. This omission is a serious inconsistency since large scale eddies must mix momentum as well as heat and moisture. Nonlocal mixing of momentum is the main subject of this thesis. Unfortunately, the transport of momentum is more complicated since it is a vector and the influence by both baroclinicity and pressure fluctuations suggests that a formulation of large eddy mixing of momentum is more difficult. Pressure fluctuations in the heated boundary layer apparently reduce the correlation between vertical and horizontal velocity fluctuations (Zilitinkevich, 1973; Bergström and Högström, 1989; Shaw *et al.* 1990). For example, Mahrt (1991a) found that thermals in the sheared boundary layer are characterized by a systematic phase lag between the vertical and horizontal velocity fluctuations leading to a low correlation coefficient and inefficient momentum transport.

Partly due to the low correlation, flux sampling criteria for the momentum flux appear to require a larger record length than that required for heat and moisture (Mahrt and Gibson, 1992; Lenschow *et al.*, 1994). As an additional complication to data analysis, the horizontal velocity seems to be affected by low frequency variations referred to as inactive eddies in Högström (1990) and Mahrt and Gibson (1992). The dynamics of these inactive eddies and their influence on the momentum flux at higher levels in the boundary layer are not well understood. Near the surface, these observed motions may be simply the large eddies whose vertical motion is

much reduced by the presence of the ground surface or they may be associated with roll vortices or transient mesoscale pressure disturbances.

The momentum flux is also influenced by baroclinicity. The study of Arya and Wyngaard (1975) suggests that convective mixing reduces the vertical gradient of mean momentum to values much smaller than the thermal wind shear. This in turn implies that the momentum flux profile is characterized by significant curvature. Brost *et al.* (1982) observed quasi-barotropic marine flows which were approximately well mixed in momentum with strong wind-induced mixing. In this case the streamwise momentum flux component was quasi-linear. More recently, Lidar observations (Piironen and Eloranta, 1993) in the heated boundary layer during FIFE 1989 (First International Satellite Land Climate Program Field Experiment; Sellers *et al.*, 1988) showed well mixed momentum profiles as well. When the boundary layer mean momentum becomes well mixed, the eddy diffusivity or any purely local scheme fails in the interior of the mixed layer where the mean gradient vanishes but the flux remains significant. As a result, the transport by the large boundary-layer eddies must be included in the mixing formulation for momentum as well as for heat and moisture.

The previous simple formulations for large eddy mixing have been primarily confined to the case of convectively driven circulations. However numerous laboratory studies of neutrally stratified boundary layers show that both longitudinal and transverse eddies lead to significant mixing on the scale of the boundary layer. Longitudinal roll vortices are known to occur under a variety of conditions in the atmosphere (Kelly, 1984; Puhakka and Saarikivi, 1986). The case of cloud streets appears to be a small subclass of roll vorticies where sufficient moisture is available and competing circulations are not present. Longitudinal vortices appear to modulate the smaller scale turbulence and flux (LeMone, 1976) and lead to significant mixing of momentum on the scale of the boundary layer (e.g., Brown and Mourad, 1990; Etling and Brown, 1993) even in the near neutral and weakly stratified cases.

Nonlocal mixing may occur in the very stable case where intermittent burst-

ing leads to destabilization of the entire boundary layer. It is not clear if such bursting consists of eddies on the scale of the boundary layer or if the mixing occurs through a sequence of smaller eddies. Unfortunately fluxes have not been adequately sampled in the very stable boundary layer and little observation evidence is available for model construction. In this study, we do not include the stable case.

# Chapter 2

# General Formulation

The various formulations for the turbulent flux at a given level $z$ is schematically shown in Fig. 2.1. Here we show possible mixing schemes for a 5-layer model and we discuss the schemes in the order shown in Fig. 2.1:

1. In the usual application of local diffusion, "direct" mixing occurs only between adjacent grid levels and only one height-dependent mixing coefficient is specified at a given grid point.

2. In the case of top-down, bottom-up diffusion (Wyngaard and Brost, 1984 and others), two height-dependent mixing coefficients are specified for a given level $z$.

3. In transilient theory (e.g, Stull, 1988) direct mixing is allowed to occur at all possible scales. All together $N(N-1)/2$ constant coefficients are required with $N$ denoting the number of grid points; for example with 5 levels in the boundary layer, 10 height independent coefficients are necessary to predict the flux at level $z$.

4. In the two-scale approach (Brown, 1982), the flux due to the large eddies is formulated as distinct from the small scale mixing. In Brown's study, the large eddies were formulated in terms of roll vortices. In principal, large eddy transport could be generalized to include all boundary-layer scale motions. With the two-scale approach, small scale diffusion occurs between adjacent grid levels and mixing by large eddies simultaneously occurs across the bulk of the boundary layer. This formulation requires two height dependent mixing coefficients.

Here we choose the two-scale mixing approach because it recognizes the lim-

| Eddy Diffusivity | Top-down, Bottom-up | Transilient Theory | Two-scale Mixing |
|:---:|:---:|:---:|:---:|
| one height-dependent coefficient | two height-dependent coefficients | 10 independent coefficients | two height-dependent coefficients |
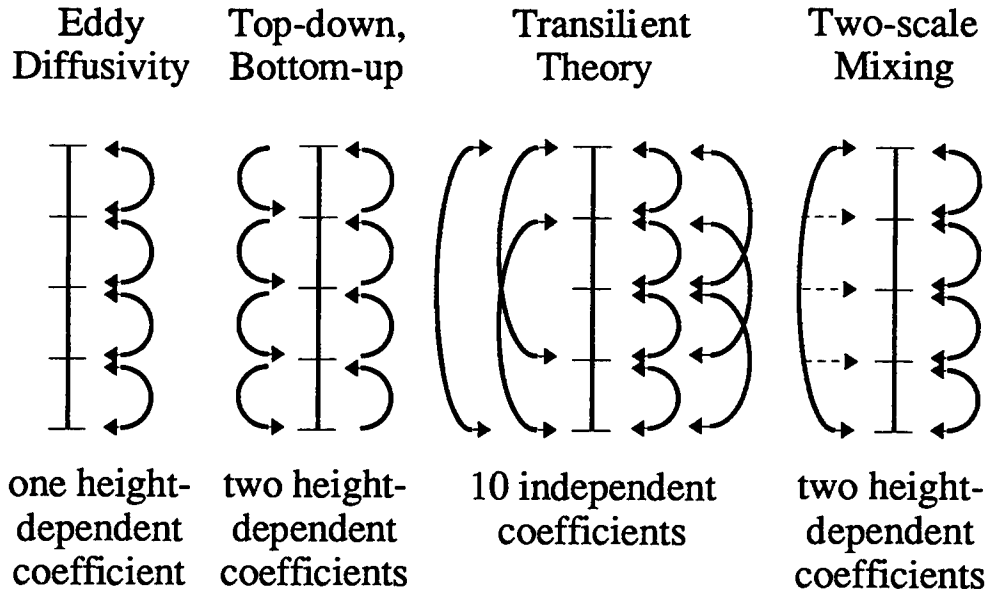
Figure 2.1: Examples of mixing schemes for a 5-layer model.

ited complexity allowed in large scale models and the fact that large eddies mix momentum in a sheared convective boundary layer (Mahrt, 1991a). This approach also accommodates comparisons with limited existing flux data in the interior of the atmospheric boundary layer. Although a simple method, the two-scale approach for momentum mixing is physically appealing since the apparent transport of momentum by boundary layer scale eddies is included explicitly. It would be inconsistent to describe the turbulent diffusion of momentum as a purely local process when at the same time large eddy transport of heat and moisture are included in a model. In other words, large scale eddies cannot in general mix heat and moisture without mixing momentum.

The local eddy diffusivity with the gradient correction will be considered as a special case of the two-scale approach. The gradient correction approaches of Priestley and Swinbank (1947), Deardorff (1972), Troen and Mahrt (1986), Holtslag and Moeng (1991) and Holtslag and Boville (1992) can be expressed in the form

$$\left(\overline{w'f'}\right) = -K_f(z)\left(\frac{\partial f}{\partial z} - \gamma_c\right) \tag{2.1}$$

where $K_f$ is the eddy diffusivity and $\gamma_c$ is a correction to the local gradient which

parameterizes the contribution of the large scale eddies to the total flux $\left(\overline{w'f'}\right)$. The variable $f$ represents heat, momentum, moisture or a passive scalar.

For heat flux, $\gamma_c$ is referred to as the "countergradient correction" since the heat flux in the interior of the well mixed boundary layer remains upward even though the local gradient becomes weakly stable. Note that specifying $\gamma_c$ is equivalent to directly specifying the height dependence of the large eddy flux to be $K_f(z)\gamma_c$. However, the height dependence of the large eddy flux is not necessarily expected to be directly proportional to the height dependence of the small scale diffusion coefficient $K_f(z)$ since the two processes are distinctly different. The large eddies mix according to the bulk gradient and are expected to scale with the boundary-layer depth and surface layer variables. Therefore, existing two-scale formulations seem somewhat inconsistent.

In this present study, we will directly formulate the large eddy flux without relating it to the small scale eddy diffusivity so that the flux at level $z$ can be expressed as

$$\left(\overline{w'f'}\right) = -K_f(z)\frac{\partial f}{\partial z} + \left(\overline{w'f'}\right)_L \qquad (2.2)$$

where $K_f$ is the mixing coefficient for the smaller scale diffusion between adjacent grid levels and $(\overline{w'f'})_L$ is the large eddy flux. This formulation can be rewritten in format (2.1) where $\gamma_c$ is determined by equation (2.1) and (2.2). The similarity formulation for $(\overline{w'f'})_L$ outlined below can also be converted to a bulk exchange coefficient and the bulk gradient between the surface layer and top of the boundary layer. Scaling the bulk exchange coefficient with the surface fluxes and depth of the boundary layer, we can formulate the large eddy stress as

$$\left(\overline{w'f'}\right)_L = S_f\left(\frac{z}{L}\right)\left(\overline{w'f'}\right)_s\left(1 - \frac{z}{h}\right)^q \qquad (2.3)$$

with

- $S_f(z/L)$: a coefficient which depends on stability; in the case of momentum it depends also on baroclinicity.

- $(\overline{w'f'})_s$: the surface flux,

- $h$: the boundary layer height,

- $q$: a constant which determines the shape of the profile function.

At the surface, $S_f(z/L)$ becomes the fraction of the flux due to the large eddies. Near the surface, $w'$ is associated with small scale motions, however it may be modulated or directly driven by the large eddy stress. As another possibility, boundary layer scale thermals may organize small thermals; as a possible result, the cospectra near the surface does not vanish at boundary layer scales (Etling and Brown, 1993). Entrainment near the boundary layer top is considered a small scale process and allotted to the small scale diffusion term in (2.2).

Although (2.2) is philosophically derived from a different point of view compared to the previous two-scale approach (2.1), the two approaches become mathematically equivalent. This is because the height dependence of the small scale local eddy diffusivity $K_f(z)$ has been formulated in terms of surface fluxes and the boundary-layer depth following the original parameterization of Brost and Wyngaard (1978). That is, the height dependence of the local eddy diffusivity follows boundary layer scaling even though it acts on the local gradient. The fact that the profile function for the large eddy transport is of the same form as that of the local eddy diffusivity cannot be justified. However, inadequacy of existing data has not allowed the separation of the two effects. Therefore, the following approach will have this possible inconsistency

Formulation (2.3) fails to include modification near the surface where the large eddy flux must decrease toward the surface and vanish at the surface. The large eddies become more two-dimensional near the ground with weaker vertical motion and less flux contribution to the total flux. As a result, the flux shifts to smaller scale local diffusion in the surface layer (Højstrup, 1982).

The simplest generalization of (2.3) which accommodates such effects would

be to include a factor $(z/h)^r$ in (2.3) which can be written in a general form as

$$\left(\overline{w'f'}\right)_L = S_f \left(\frac{z}{L}\right) \left(\overline{w'f'}\right)_s \left(\frac{z}{h}\right)^r \left(1 - \frac{z}{h}\right)^q \tag{2.4}$$

This formulation allows the decrease of $(\overline{w'f'})_L$ toward the surface and becomes zero at the surface.

Momentum flux is more complex since $f$ is a vector. An assumption must be made about the variation of the large eddy stress direction with height. We will assume that the large eddy stress vector is aligned with the bulk shear vector between the top of the surface layer and the layer just below the boundary-layer top. This formulation is considered in more detail in Chapter 4.

# Chapter 3

# Nonlocal Mixing of Heat

## 3.1 Introduction

This section summarizes the existing two-scale approach for the turbulent mixing of heat in a simple one-dimensional atmospheric boundary model based on first order closure. First we discuss the nonlocal mixing formulation for heat given in Troen and Mahrt (1986) and which has been modified by Holtslag and Boville (1992). We then show a data comparison that illustrates how a two-scale approach for heat performs in a simple boundary layer model. This approach for heat is extended to the case of momentum mixing in the next section.

## 3.2 Modeling the Heat Flux

We consider the so called "countergradient correction" for the nonlocal heat flux in the prognostic equation for temperature in a 1-D model. The nonlocal heat flux in a convective boundary layer is formulated by specifying a heat flux profile which is a function of the local eddy diffusivity and scaling variables relevant for an unstable boundary layer.

The prognostic equation for temperature can be simplified to a diffusion equation where the nonlocal contribution is included as a gradient correction. The simplified prognostic equation is:

$$\frac{\partial \Theta}{\partial t} = \frac{\partial}{\partial z} \left( K_h \left( \frac{\partial \Theta}{\partial z} - \gamma_\Theta \right) \right) - w \frac{\partial \Theta}{\partial z} \qquad (3.5)$$

with

- $\Theta$: the potential temperature,

- $K_h$: the eddy diffusivity for heat,

- $\gamma_\Theta$: the gradient correction,

- $w$: large scale vertical motion.

Following the formulation of Holtslag and Boville (1992), the gradient correction for heat can be written as:

$$\gamma_\Theta = C \frac{w_*(\overline{w'\Theta'})_s}{w_s^2 h} \tag{3.6}$$

with

- $(\overline{w'\Theta'})_s$: surface heat flux,

- $w_s$: boundary layer velocity scale, a function of the convective velocity scale $w_*$ $(m/s)$ and the surface friction velocity $u_*$ $(m/s)$.

- $h$: boundary layer height

- $C$: a constant set to 7.2

The velocity scale $w_s$ is defined as:

$$w_s = \left(u_*^3 + 0.6w_*^3\right)^{\frac{1}{3}} \tag{3.7}$$

By defining this velocity scale, shear generation of turbulence in the heated boundary layer is considered. In the free convection limit, when turbulence is buoyancy generated, $w_s$ is a function of the convective velocity scale $w_*$ only.

The eddy diffusivity for heat is defined as (Troen and Mahrt, 1986):

$$K_h(z) = w_s Pr^{-1} kh \left(\frac{z}{h}\right)^r \left(1 - \frac{z}{h}\right)^p \tag{3.8}$$

with

- $k$: the von Kármán constant

- $r$: set to be 1

- $p$: normally set to be 2

- $Pr$: the Prandtl number

The Prandtl number $Pr$ is defined as

$$Pr = \left( \frac{\Phi_h \left( \frac{z}{L} \right)}{\Phi_m \left( \frac{z}{L} \right)} + Ck\frac{z}{h} \right)_{z=z_s} \tag{3.9}$$

evaluated at the top of the surface layer $z_s$; the nondimensional profile functions for the gradients of shear $\Phi_m$ and temperature $\Phi_h$ are defined in Ek and Mahrt (1991).

We rewrite the prognostic equation (3.5) and write the turbulent heat flux in the form described by equation (2.2). The prognostic equation (3.5) becomes

$$\frac{\partial \Theta}{\partial t} = \frac{\partial}{\partial z} \left( K_h \frac{\partial \Theta}{\partial z} \right) - \frac{\partial}{\partial z} \left( \overline{w'\Theta'} \right)_L - w\frac{\partial \Theta}{\partial z} \tag{3.10}$$

where the nonlocal heat flux is expressed explicitly. The nonlocal flux of heat can be expanded as (Holtslag and Moeng, 1991)

$$\left( \overline{w'\Theta'} \right)_L = K_h(z) \cdot \gamma_\Theta \tag{3.11}$$

$$= w_s Pr^{-1} kh \left( \frac{z}{h} \right) \left( 1 - \frac{z}{h} \right)^2 C \frac{w_* (\overline{w'\Theta'})_s}{w_s^2 h} \tag{3.12}$$

This form of the nonlocal flux can be compared with the form given in equation (2.4). Equating (2.4) and (3.12), the stability coefficient $S_\Theta(z/L)$ is

$$S_\Theta \left( \frac{z}{L} \right) = Pr^{-1} Ck \frac{w_*}{w_s} \tag{3.13}$$

if we assume that $q = 2$ and $r = 1$ in (2.4).

## 3.3  Data Comparison

Using (3.10) we simulate 28 July 1989 during FIFE which is a typical convective summer day. The simulation starts at 0700 LST (Local Standard Time) and is integrated until 1200 LST. The data and the model run is described in more detail
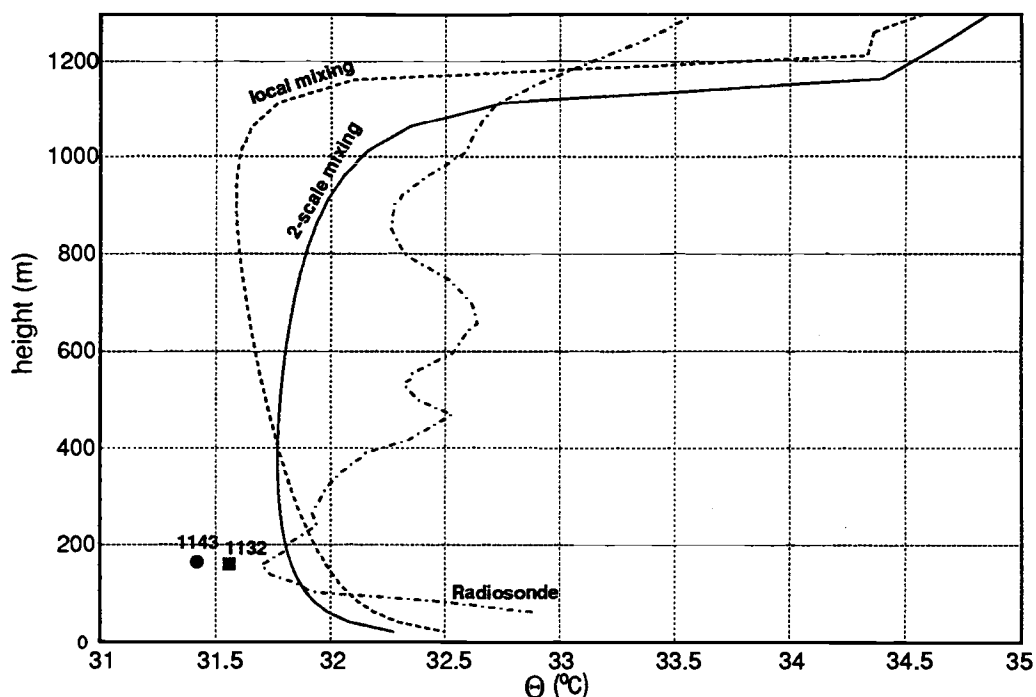
Figure 3.1: Predicted potential temperature (°C) profile for 28 July 1989 at 1200 LST during FIFE with two-scale mixing versus local mixing. Symbols show aircraft flux measurements with the corresponding start time (LST) of the flight leg. The radiosonde was launched at 1130 LST.

in Section 4.3. The radiosonde profile shows the characteristic potential tempera-ture profile of a convective boundary layer although there are perturbations in the sounding profile especially between 400-800 m (Fig. 3.1). The radiosonde might be caught in a thermal in this layer. We find the slightly stable stratification charac-teristic for the upper part of a convective boundary layer. The "classic" potential temperature profile of the convective boundary layer is predicted by the two-scale approach: with a superadiabatic surface layer, a mixed layer region with weak ver-tical gradient and a slightly stable potential temperature profile in the upper part of the boundary layer. In contrast, the local mixing scheme fails to predict these characteristics and the potential temperature profile remains unstable throughout the boundary layer. The radiosonde and the aircraft measurements agree well with the profile predicted by two-scale approach.

The predicted total heat fluxes are in good agreement with the aircraft mea-surements (Fig. 3.2). The nonlocal flux reaches a maximum in the interior of the
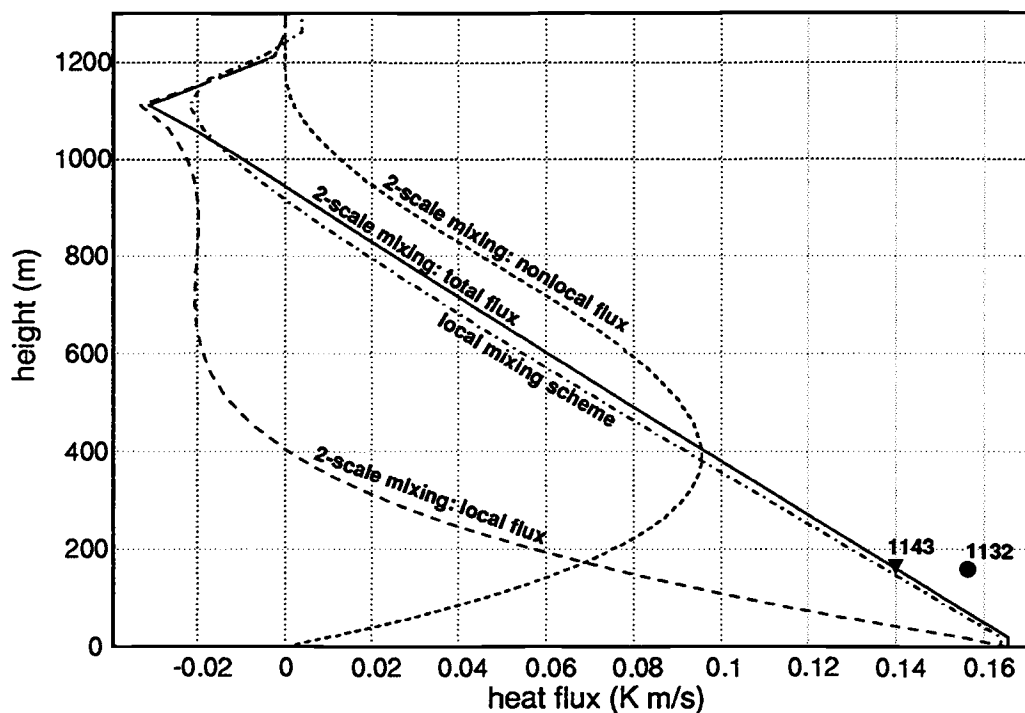
Figure 3.2: Predicted heat flux profile ($K$ m/s) for 28 July 1989 at 1200 LST during FIFE. The two-scale mixing scheme with the total flux = local + nonlocal heat flux versus the heat flux predicted by a local mixing scheme alone. Symbols show aircraft heat flux measurements (see also Fig. 3.1).

boundary layer where the local flux is roughly one third of the nonlocal flux. The local flux is dominant in the lower one third of the boundary layer where the non-local flux becomes small. Both the local and nonlocal fluxes approach zero at the boundary layer top. The nonlocal flux is positive throughout the boundary layer and decreases quasi-linearly from its maximum to the boundary layer top. The local flux contribution to the total flux is negative throughout the upper three quarters of the boundary layer (Fig. 3.2) reflecting the downgradient diffusion due to the stable stratification of the potential temperature profile (Fig. 3.1). But this down-gradient diffusion is exceeded by the nonlocal flux in this region. Downward local mixing dominates in the entrainment region. We find that the parameterization for the nonlocal flux (3.12) in combination with the local flux profile satisfies the assumption that the entrainment flux is dominated by local diffusion. Combining these two flux contributions we predict the usual linear heat flux profile (Fig. 3.2).

# Chapter 4

# Nonlocal Mixing of Momentum

## 4.1  Introduction

In this section the parameterization for the nonlocal turbulent flux of momentum is examined. We will present model results testing the proposed formulation from Chapter 2 in a simple boundary layer model under several different atmospheric conditions.

The motivation for this development is based on Lidar observations (Piironen and Elorenta, 1993) which show well-mixed momentum in the heated atmospheric boundary layer during FIFE 1989. The Lidar observations of well mixed momentum suggest that a nonlocal flux of momentum needs to be incorporated in a boundary layer model since a local gradient-flux relationship obviously cannot produce well mixed momentum. Momentum profiles observed from balloon and aircraft soundings generally do not show well mixed momentum. This may be due to inadequate sampling associated with low frequency oscillations of the wind field.

A simple scaling argument for the expected stress, wind and geostrophic wind profiles in a convective boundary layer suggests that a convective boundary layer in the presence of shear is not likely to support strong vertical gradients in the velocity profile even with baroclinic conditions (Arya and Wyngaard, 1975). We consider the steady-state mean shear equation in the general form (the mean momentum equation differentiated with respect to $z$):

$$\frac{\partial^2 \overline{w'u'}}{\partial z^2} = f\left(\frac{\partial v}{\partial z} - \frac{\partial v_g}{\partial z}\right) \tag{4.14}$$

$$\frac{\partial^2 \overline{w'v'}}{\partial z^2} = f \left( \frac{\partial u_g}{\partial z} - \frac{\partial u}{\partial z} \right) \tag{4.15}$$

From equations (4.14) and (4.15) we find that a well mixed momentum profile $(\partial \vec{u}/\partial z \approx 0)$ implies a linear stress profile under barotropic conditions $(\partial \vec{u}_g/\partial z = 0)$. The baroclinic case $(\partial \vec{u}_g/\partial z \neq 0)$ is more complicated . If we assume that the mean wind shear is on the same order of magnitude as the geostrophic shear, equations (4.14) and (4.15) imply that the stress profile curvatures are approximately zero. However, a significant gradient in the mean wind profile is likely to interact with the vertical variance $\overline{w'^2}$ , leading to the production of momentum flux. To illustrate this we write the simplified budget equation for the tendency of the turbulent momentum flux $\overline{w'u'}$ (see e.g. Stull, 1988, p. 137 ff) assuming horizontal homogeneity and neglecting subsidence:

$$\frac{\partial \overline{w'u'}}{\partial t} = -\overline{w'^2}\frac{\partial \overline{u}}{\partial z} - \frac{\partial \left( \overline{u'w'w'} \right)}{\partial z} + \frac{g\overline{u'\Theta_v'}}{\overline{\Theta_v}} + \overline{\frac{p'}{\varrho} \left( \frac{\partial u'}{\partial z} + \frac{\partial w'}{\partial x} \right)} - 2\epsilon_{uw} \tag{4.16}$$

The first term on the r.h.s. is the production of momentum flux by the mean wind shear, the second term represents turbulent diffusion of $\overline{w'u'}$ by the turbulent fluctuation $w'$, the third term is the buoyancy production/consumption, the fourth term is the return-to-isotropy term and the last one is the dissipation term. For a convective boundary layer we can assume a simplified stationary budget for the momentum flux assuming an approximate balance between the first and fourth term in (4.16). The buoyancy production/consumption and turbulent diffusion term are approximately on the same order of magnitude with opposite signs and are therefore not considered in this simplified budget (Therry and Lacarrère, 1983). The interaction of the vertical velocity variance and the mean gradient is not expected to vary linearly with height in a typical convective boundary layer and thus generates curvature of the stress profile in contradiction to the above test hypothesis for equations (4.14) and (4.15) (Stull, 1988; Therry and Lacarrère, 1983). We realize that this simplified budget for the momentum flux is perhaps only valid in certain stability regimes. Furthermore we have to note that the arguments for the simplified budget for the momentum flux are based on results obtained from a third-order

turbulence closure scheme model. We have to be aware of uncertainties due to closure assumptions. But the expectation of weak gradients in the mean wind profile under convective conditions is supported by some observations (e.g. Wangara Day 33 discussed in Arya and Wyngaard, 1975). As additional evidence the velocity defect in a boundary layer seems to show no significant dependence on baroclinicity under unstable conditions (Garratt, 1992). The velocity defect is mainly affected by stability.

The previous discussion leads to the dependence of the stress profile curvature on the geostrophic shear (or baroclinicity) rewriting (4.14) and (4.15) for convective conditions:

$$\frac{\partial^2 \overline{w'u'}}{\partial z^2} \approx -f \frac{\partial v_g}{\partial z} \tag{4.17}$$

$$\frac{\partial^2 \overline{w'v'}}{\partial z^2} \approx f \frac{\partial u_g}{\partial z} \tag{4.18}$$

implying that $\partial u/\partial z$ and $\partial v/\partial z \approx 0$.

In summary, weak or vanishing gradients in the components of the mean wind profile are expected for the barotropic and the baroclinic convectively mixed boundary layer (Arya and Wyngaard, 1975), although the evidence of the influence of baroclinicity on the velocity profiles is somewhat circumstantial. Furthermore, the curvature of the stress profile is determined by the geostrophic shear.

## 4.2   Formulation

We express the nonlocal flux of momentum in the form proposed in (2.4). The formulation for the nonlocal flux of momentum in a sheared and unstable boundary layer is expected to scale with the friction velocity $u_*$, the convective velocity scale $w_*$ and the boundary layer height $h$.

Here, $f$ in (2.4) becomes a vector and it is assumed that the large eddy stress is aligned with the bulk shear vector. We calculate the bulk shear vector as the difference between the wind vectors at the top of the surface layer and at the

model level just below the boundary layer top. Furthermore, we assume that the large-scale momentum flux is of the same sign throughout the boundary layer.

We propose following form for (2.4) (here the $x$-component of the large eddy stress):

$$\left(\overline{w'u'}\right)_L = -S_m u_*(w_* + u_*)\left(\frac{z}{h}\right)^r \left(1 - \frac{z}{h}\right)^q \frac{u_{sh}}{|\vec{v}_{sh}|} \tag{4.19}$$

with

- $S_m$: an adjustable coefficient,

- $u_*$: the surface friction velocity $(m/s)$,

- $w_*$: the convective velocity scale $(m/s)$,

- $u_{sh}$: the $x$-component of the bulk shear vector,

The $y$-component assumes an analogous form. The large eddy flux scales with the surface stress $u_*^2$ for the neutral limit $(w_* \to 0)$. In the free convection limit $(u_* \to 0)$, the large eddy flux becomes zero. This reflects the fact that the correlation between the velocity perturbations $u'$ and $w'$ becomes small with increasing instability (Mahrt, 1991a). The proposed formulation for the nonlocal flux includes a stability dependence based on $w_*$. The coefficient $S_m$ is a parameter to be adjusted against data and is expected to be a function of baroclinicity. To be consistent with the parameterization for the nonlocal flux of heat (see equation (3.12)) we use the profile function $(z/h)(1 - z/h)^2$. This profile function successfully describes the height dependence of the large eddy heat flux (see e.g. Figs.3.1 and 3.2).

The two horizontal components of the prognostic equation for momentum at level $z$ in the 1-D model is written as

$$\frac{\partial u}{\partial t} = f(v - v_g) - w\frac{\partial u}{\partial z} + \frac{\partial}{\partial z}\left(K_m\frac{\partial u}{\partial z}\right) - \frac{\partial}{\partial z}\left(\overline{w'u'}\right)_L \tag{4.20}$$

$$\frac{\partial v}{\partial t} = f(u_g - u) - w\frac{\partial v}{\partial z} + \frac{\partial}{\partial z}\left(K_m\frac{\partial v}{\partial z}\right) - \frac{\partial}{\partial z}\left(\overline{w'v'}\right)_L \tag{4.21}$$

with

- $f$: the Coriolis parameter,

- $v_g$ and $u_g$: the geostrophic wind components;

- $w$: the large scale vertical motion,

- $K_m$: the eddy diffusivity for momentum.

The local eddy diffusivity for momentum in an unstable boundary layer is defined as (Troen and Mahrt, 1986):

$$K_m(z) = w_s k h \left(\frac{z}{h}\right)^r \left(1 - \frac{z}{h}\right)^p \tag{4.22}$$

with $r = 1$ and $p = 2$.

## 4.3   The Data

We compare model results with observational data from FIFE 1989. Mean wind profiles are obtained from the University of Wisconsin Volume Imaging Lidar during FIFE (Piironen and Eloranta, 1993). The Lidar recorded the spatial aerosol scattering over the Konza prairie between 26 July and 11 August 1989. The Lidar records scattered signals from a $\sim 100$ km$^3$ volume over an area of $\sim 15 \times 6$ km$^2$ with a spatial resolution of $\sim 15$ - $100$ m and a temporal resolution of $\sim 3$ min/scan. Wind speed and direction were estimated by measuring the drift of aerosol back scattering patterns inside successive Lidar images, using a two-dimensional spatial cross correlation technique described in Schols and Eloranta (1992). We use time- and volume-averaged Lidar wind profiles for our data comparisons, where wind profiles represent one hour means. We also compare the predicted momentum profiles with Twin Otter aircraft data (MacPherson et al., 1992, Eloranta and Forrest, 1992) and radiosonde profiles. In general, Lidar wind profiles provide the best data set to compare with predicted mean wind profiles. In contrast radiosonde data contain no averaging, and aircraft data are horizontal line measurements and sometimes contain inadequate averaging (Grossman, 1992; Mahrt and Gibson, 1992).
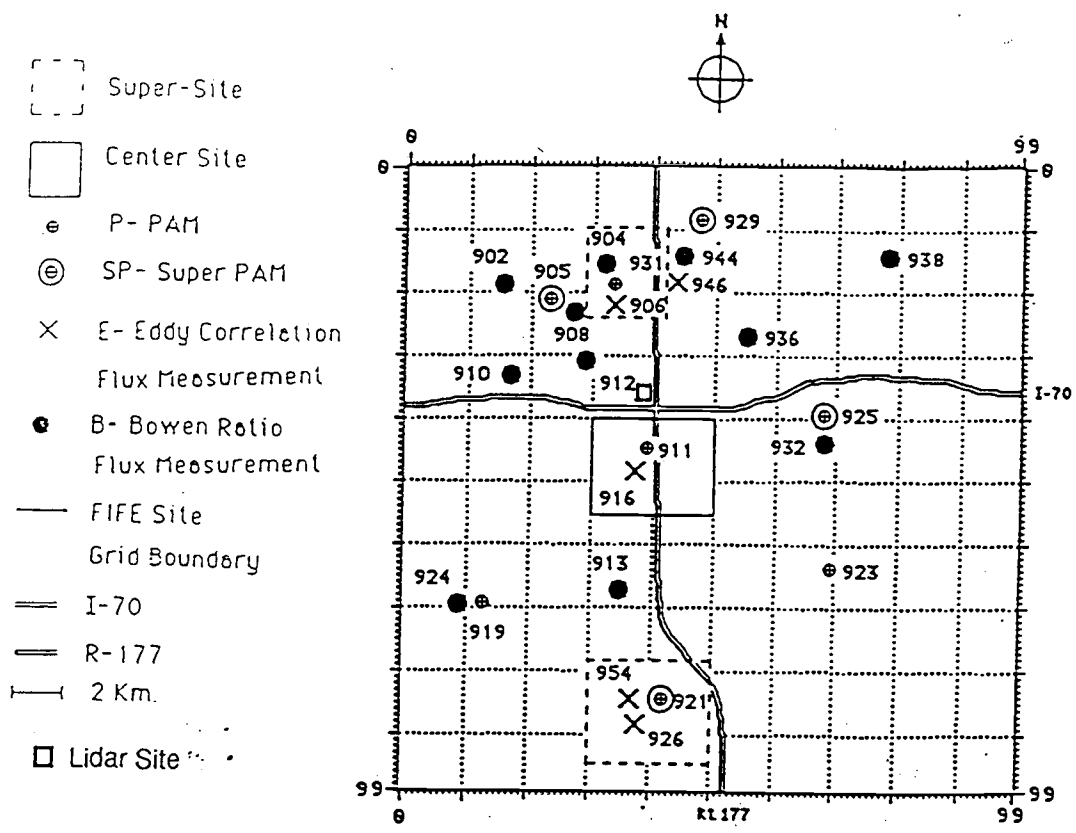
Figure 4.1: FIFE 1989 domain showing flux stations (even numbers), PAMs (Portable Automated Mesonet, odd numbers) and the Lidar site (open square) (Sellers *et al.*, 1992). The Lidar pointed south-west.
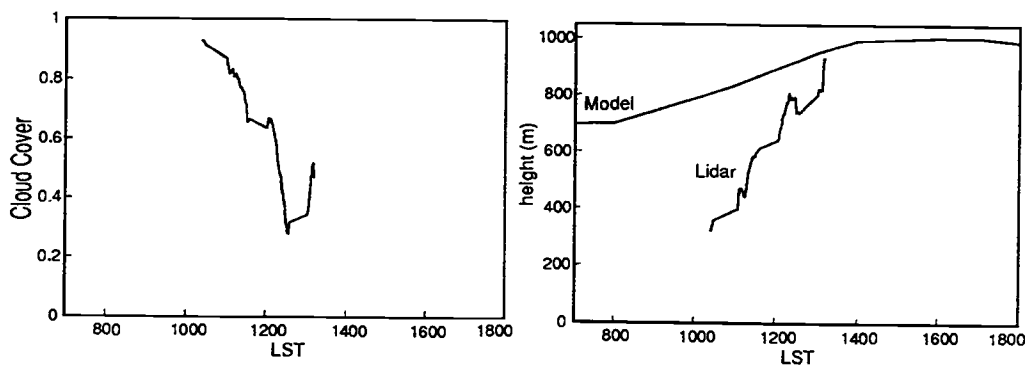


Figure 4.2: Fractional cloud cover and boundary layer height $h$ for 3 August 1989 during FIFE obtained from the Lidar. The right figure also shows the model predicted $h$.
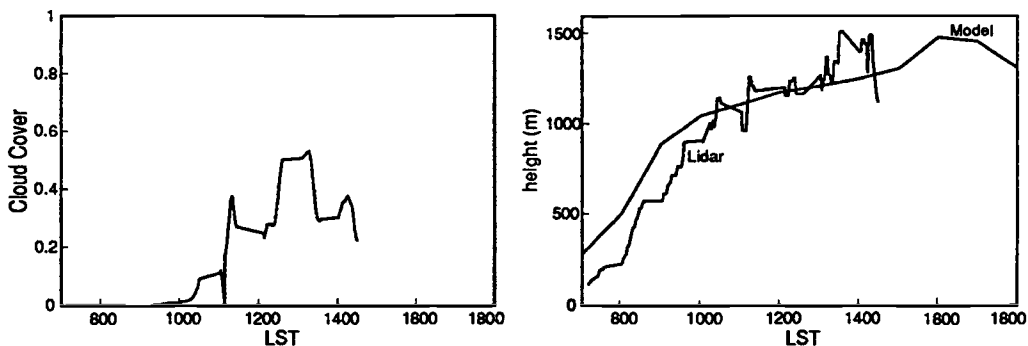
Figure 4.3: Fractional cloud cover and boundary layer height $h$ for 28 July 1989 during FIFE obtained from the Lidar. The right figure also shows the model predicted $h$.

The estimated mean boundary layer height and cloud cover are also available from this Lidar dataset. Figs. 4.2 and 4.3 show the cloud cover and the mean boundary layer height obtained from Lidar data for 3 August and 28 July 1989, respectively. The cloud cover algorithm used by Piironen and Eloranta (1993) is reliable for small cloud cover. Potential errors have to be expected for high cloud cover (e.g. breaks in a cloud deck) and in the case of variable cloud base levels in the scanned domain.

To help isolate errors due to the diffusion parameterization in the model, we prescribe the observed Lidar fractional cloud cover in the model. Cloud cover reduces the incoming solar radiation available for surface heating. We do not account for any modification of the turbulent mixing due to clouds (e.g. radiative effects, buoyancy driven turbulent mixing due to latent heat release). The horizontal advection terms for the boundary layer heat and moisture budget appear to be important based on radiosonde soundings for 28 July and 3 August 1989. Since horizontal advection terms are not included in the governing prognostic equations for heat, moisture and momentum in the 1-D model, predicted variables like cloud cover would be affected by omission of these terms which in turn affects the surface energy balance as a feedback effect. We crudely account for advection by "updating" the initial temperature and moisture sounding above 1000 m utilizing sounding data. In the present case study the increase of stratification due to advection reduces the
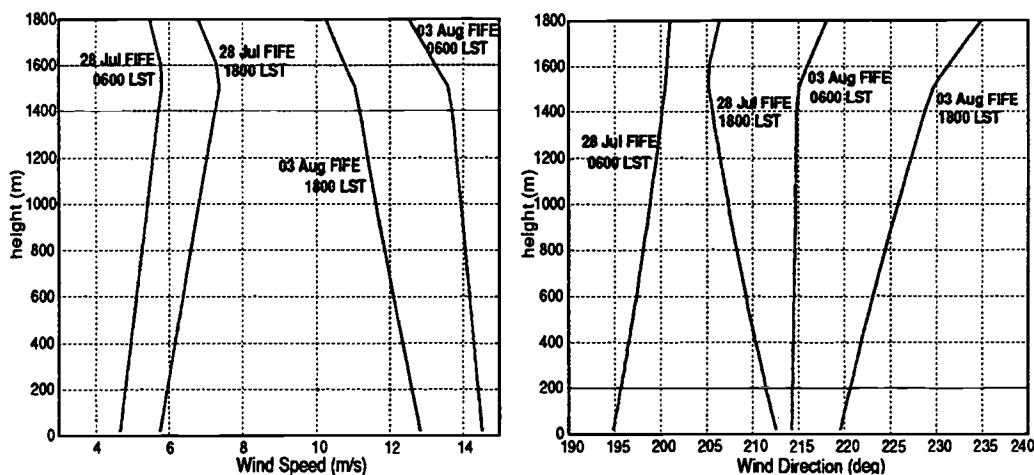
Figure 4.4: Calculated geostrophic wind speed (m/s) and direction (deg) from NMC data.

growth of the boundary layer in the afternoon.

Unfortunately, geostrophic wind profiles are not available from FIFE 1989 and are difficult to determine accurately. We use NMC upper air grid data to estimate the geostrophic winds. The NMC upper air grid data is extracted from the NOAA operational analysis system. There are four grid points in 381 km polar-stereographic projection over the FIFE area. Using additional surrounding grid-points we produce pressure height maps for 1000, 850 and 700 hPa. We calculate the horizontal pressure gradients over the FIFE site in finite difference form and estimate the geostrophic wind at these three levels. We linearly interpolate with height between the calculated geostrophic winds to estimate the profile. This method is somewhat crude and errors of the geostrophic wind due to the approximation of the pressure gradient in finite difference form and from the linear interpolation may be several meters per second.

The NMC upper air grid point data are available in 12 hour intervals. We calculated the geostrophic wind profiles for 0600 and 1800 LST and interpolated them linearly in time to determine the geostrophic wind for the time period in the model simulation. Fig. 4.4 shows the calculated geostrophic wind profiles for the 3 August and 28 July 1989 during FIFE.

We initialize the model temperature and moisture profiles with radiosonde

Table 4.1: Initial model parameters for 3 August 1989

| Variable | Numerical value |
|---|---|
| large scale $w$ | max. -1 cm/s at 3000 m |
| Latitude | 39.06 N |
| Longitude | −96.33 W |
| Surface pressure | 967.2 hPa |
| Shortwave albedo | 0.2 |
| Soiltype | Silty clay loam |
| Canopy resistance (const.) | 80 s/m |
| Shading factor | 0.8 |
| volumetric soil water content upper layer 0 - 5 cm | 0.35 |
| volumetric soil water content lower layer 5 -100 cm | 0.30 |
| Roughness length for momentum (const.) | 0.01 m |
| Roughness length for heat (const.) | 0.001 m |

data. The calculated geostrophic wind profiles are used to initialize the model winds for the data comparison in order to avoid strong inertial oscillations.

## 4.4   Data Comparison

**3 August 1989**: 3 August 1989 is a day with nearly stationary wind speed on the order 10 m/s. Parameters needed for the simulation are listed in Table 4.1. The data are obtained from the FIFE Information System (FIS, Strebel *et al.*, 1990). The prescribed subsidence increases linearly with height from the surface reaching a maximum subsidence of - 1 cm/s at 3000 m. The subsidence was tuned
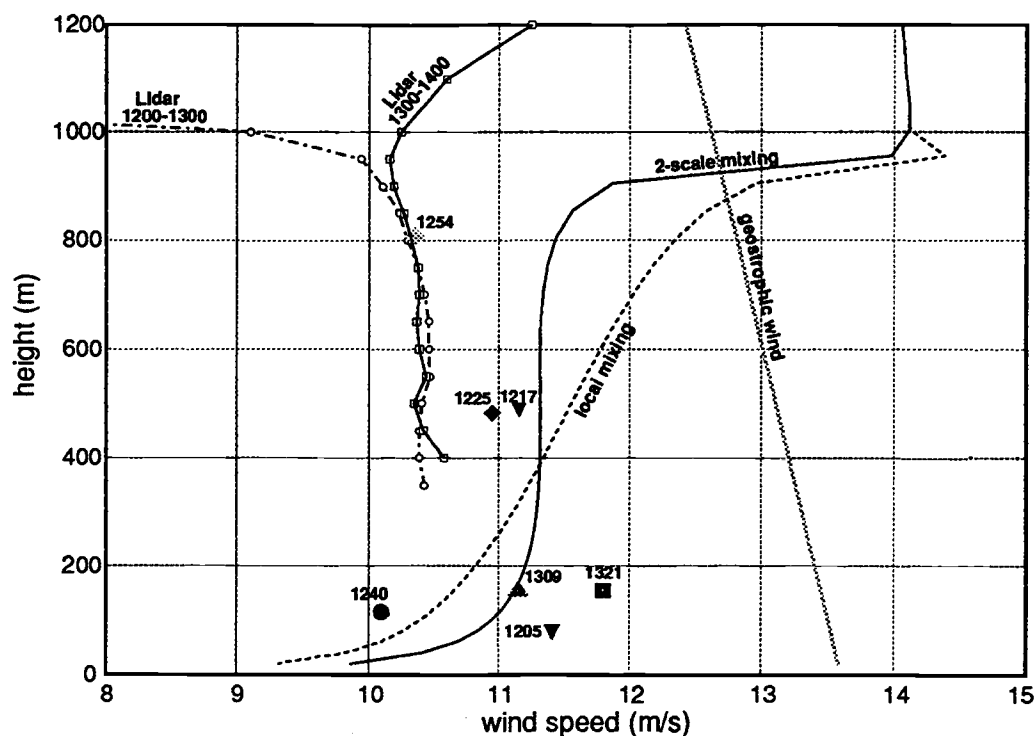
Figure 4.5: Model-predicted and observed wind speed (m/s) for 3 August 1989 at 1300 LST during FIFE: individual symbols show aircraft data indicated by the start time (LST) of the flight leg ($\sim$ 15 km long). Each aircraft data point represents a leg-average (Eloranta and Forrest (1992)). Lidar wind profiles represent one-hour averages. The winds derived from Lidar data are unreliable below 400 m and are therefore omitted.

to approximate the observed boundary layer depth in order to help isolate errors due to the mixing scheme.

We use $S_m = 1.4$ for this data comparison with the coefficient determined from sensitivity tests. The choice of this coefficient is determined in comparison with Lidar data (Section 4.5). The profiles of wind speed and direction are compared with observational data at 1300 LST. The boundary layer height is predicted to be 953 m compared to the diagnosed $\sim$ 750 m from Lidar observations (Fig. 4.2) (see Appendix C for a further discussion).

The Lidar wind speed profile (Fig. 4.5) indicates that the wind field is well mixed up to the boundary layer top. The two-scale approach leads to a well mixed profile throughout the boundary layer and agrees well with the Lidar profiles con-
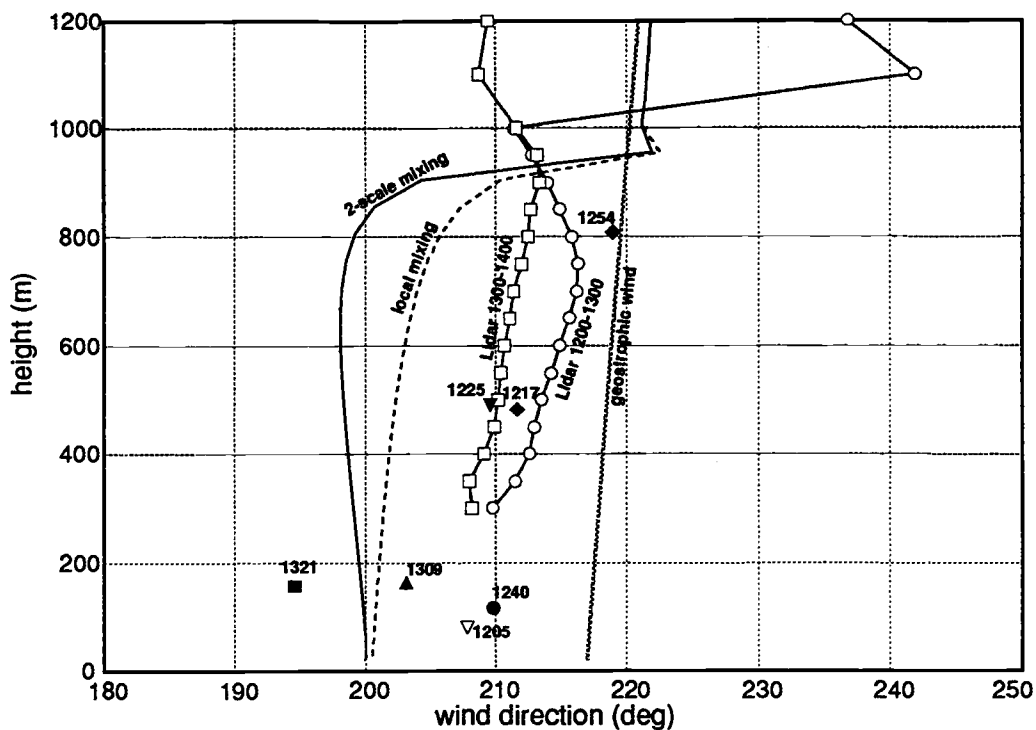
Figure 4.6: Model-predicted and observed wind direction (deg) for 3 August 1989 at 1300 LST during FIFE: individual symbols show aircraft data. The Lidar wind profiles below 400 m are not shown (see comments in Fig. 4.5)

sidering the uncertainties related to the estimation of the geostrophic wind. The wind speed predicted by the two-scale mixing scheme is $\sim 0.9$ m/s stronger than the Lidar wind speed. The local scheme predicts continuous shear throughout the boundary layer and fails to predict the observed well mixed mean momentum profile. The difference in wind speed between the two-scale approach and the local scheme is about 0.5 m/s at the first model level (20 m). The local scheme predicts a $\sim 2$ m/s higher wind speed near the boundary layer top in comparison to the Lidar data. The error due to the local diffusion scheme appear to be larger in this region.

The wind directions predicted by the two mixing schemes agree well with the Lidar and aircraft data considering the uncertainties related to the estimation of the geostrophic wind (Fig. 4.6).

The profiles of wind speed and direction for 3 August 1989 from 1100 to

1700 LST (Fig. 4.7) show that the two-scale approach leads to well mixed profiles throughout the day while the local scheme predicts significant shear. We find a slight decrease in wind speed with height for the profile predicted by the two-scale approach at 1500 LST which is probably related to the time dependence of the baroclinicity and the use of constant $S_m$. However, the decrease of wind speed with height is quite small and the scaling of the nonlocal flux by $u_*$ and $w_*$ represents the expected diurnal variation of the stress profiles reasonably well.

Aircraft observations are the only available source for stress data for 3 August 1989 in FIFE. We do not obtain a continuous stress profile from these measurements which would be desirable in order to see the shape of the profile under baroclinic conditions. The $\overline{v'w'}$-component contains most of the total stress (Fig. 4.8). The profiles for the local and nonlocal scheme are almost linear and the weak curvature of $\overline{v'w'}$ (see (4.18)) may be related to the weak baroclinicity. The two-scale approach predicts stronger surface stress compared to the local scheme which can be inferred from the predicted wind speed profiles. We found a higher wind speed at the first model level with the parameterized effect of large eddies. The surface stress is determined by a drag law which is quadratically proportional to the first model level wind speed and is multiplied by the drag coefficient. Therefore, we expect a stronger surface stress with nonlocal mixing (Fig. 4.8). The surface stress values for both schemes are listed in Table 4.3. We find that the new scheme leads to an increase of the surface stress by 10%. The stress profiles predicted by the two-scale approach compare surprisingly well with the aircraft flux data. This could be coincidental considering the uncertainties in the observed stress profile.

**28 July 1989**: We also test the proposed formulation (4.19) by modeling 28 July 1989 in FIFE. Initial parameters are listed in Table 4.2. The value $S_m = 0.8$ for the nonlocal flux parameterization produces the best results for 28 July 1989. We analyze the predicted profiles for wind speed, its components and direction at 1200 LST (we choose this time because of the availability of radiosonde, aircraft and Lidar data). The model predicts a boundary layer height of 1175 m and a mean
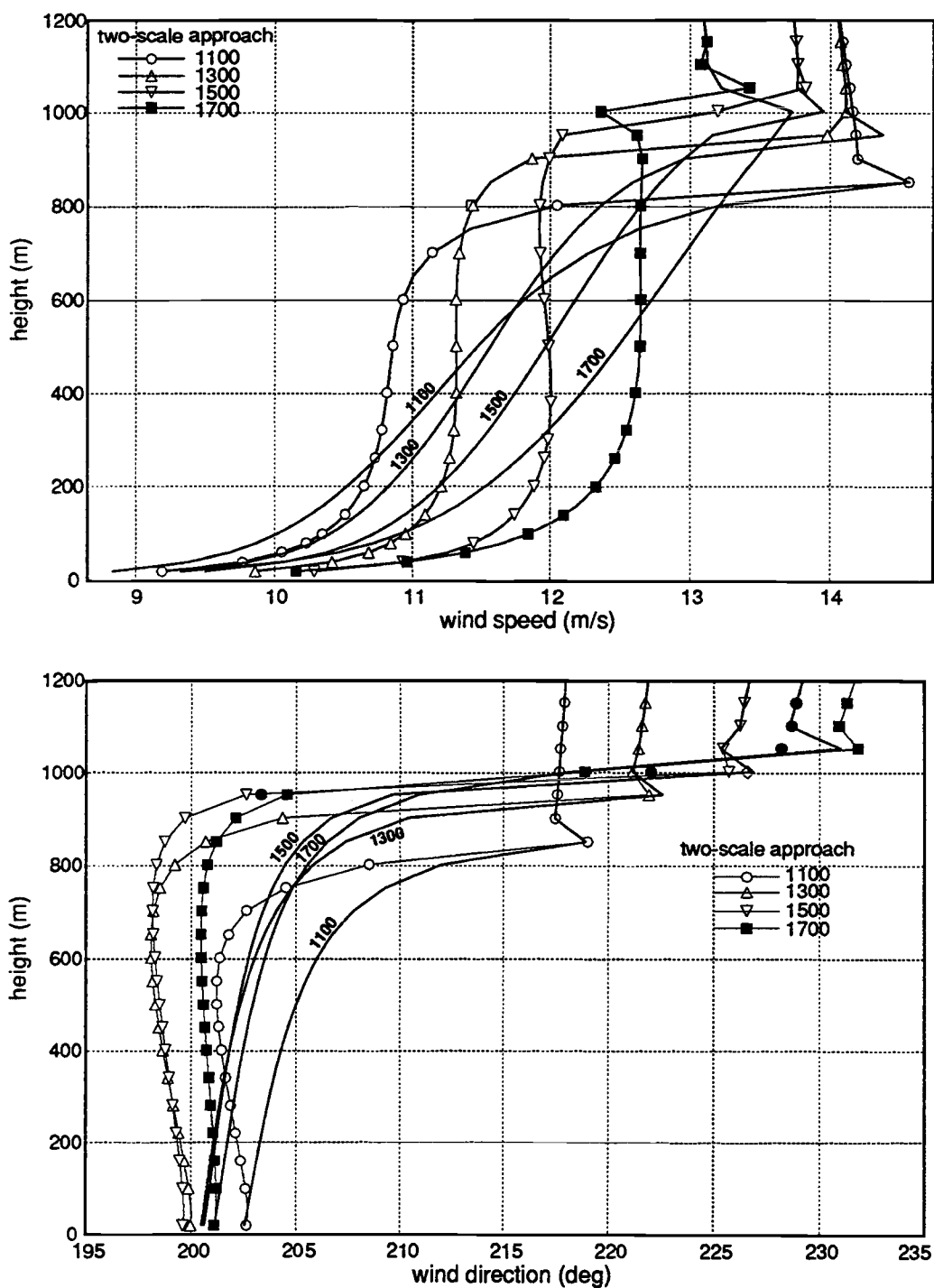
Figure 4.7: Model-predicted wind speed (m/s, top figure) and wind direction (deg, bottom figure) for 3 August 1989 during FIFE: Two-scale approach (solid lines with symbols) and local scheme (solid lines). Each profile is labelled with the corresponding time (LST).
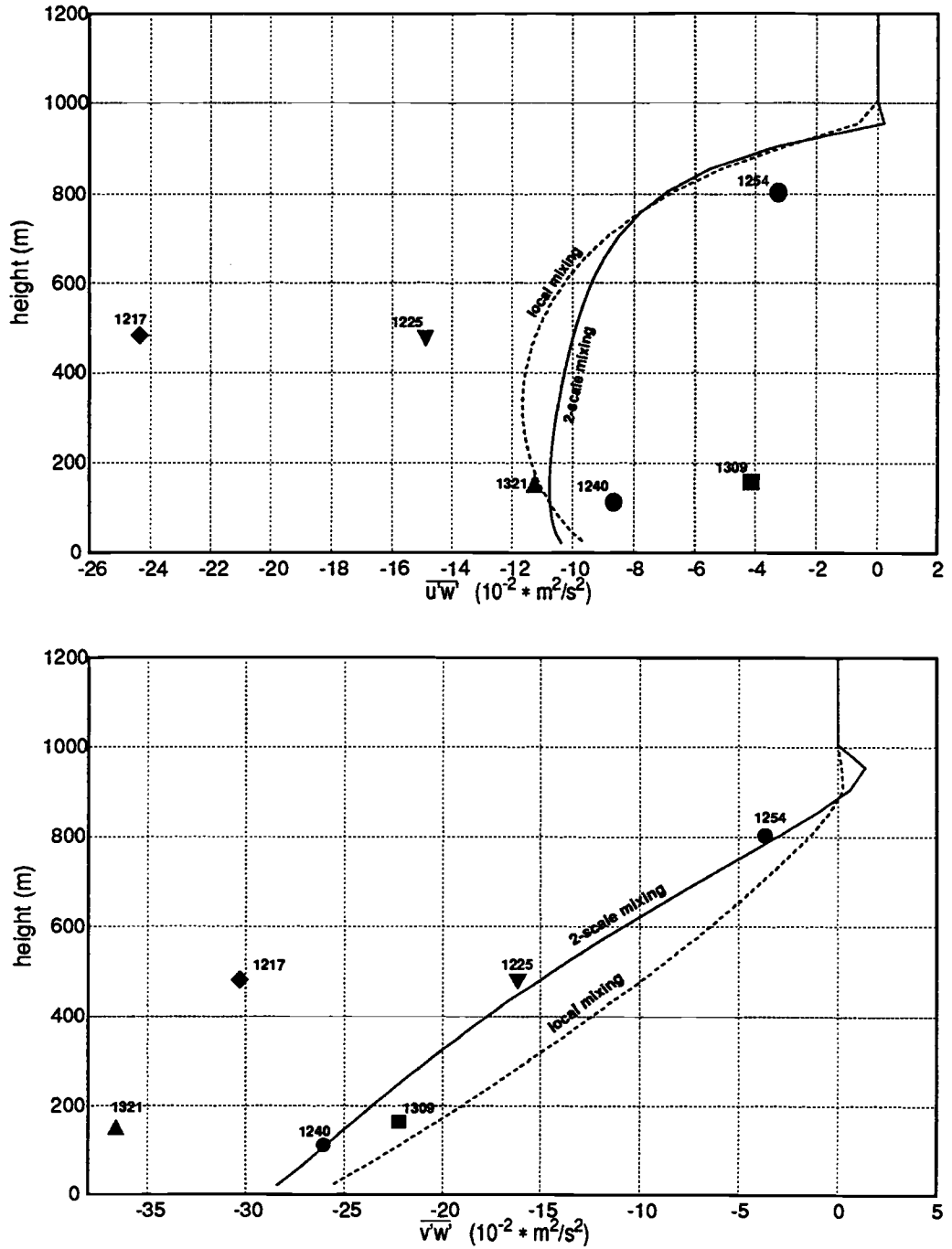
Figure 4.8: The components of the stress profile $(m^2/s^2)$ for 3 August 1989 at 1300 LST during FIFE. Top figure, $\overline{u'w'}$; bottom figure, $\overline{v'w'}$. The aircraft flux values are indicated by the corresponding start time of the flight leg (LST).

Table 4.2: Initial model parameters for 28 July 1989

| Variable | Numerical value |
|---|---|
| large scale $w$ | max. $-2$ cm/s at 3000 m |
| Latitude | 39.06 N |
| Longitude | $-96.33$ W |
| Surface pressure | 978 hPa |
| Shortwave albedo | 0.2 |
| Soil type | Silty clay loam |
| Canopy resistance (const.) | 150 s/m |
| Shading factor | 0.8 |
| volumetric soil water content upper layer 0 - 5 cm | 0.20 |
| volumetric soil water content lower layer 5 - 100 cm | 0.255 |
| Roughness length for momentum (const.) | 0.01 m |
| Roughness length for heat (const.) | 0.001 m |
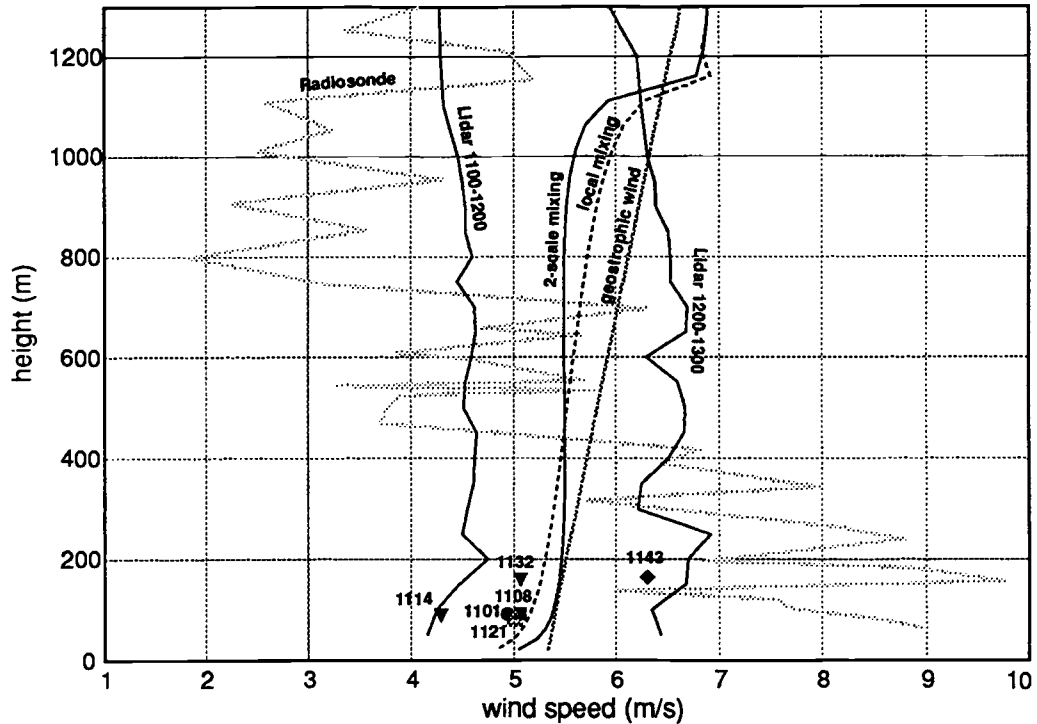
Figure 4.9: Model-predicted and observed wind speed (m/s) for 28 July 1989 at 1200 LST during FIFE: individual symbols show aircraft data indicated by the start time (LST) of the flight leg. The Lidar wind profiles represent one hour averages.

boundary-layer height is diagnosed near $\sim 1150$ m from Lidar data (Fig. 4.3).

The two-scale approach leads to a well mixed wind profile, while the local scheme shows continuous weak shear throughout the boundary layer (Fig. 4.9). For this case the differences between the two-scale and local approach are not as large as on 3 August 1989. We again find that the Lidar wind speed profile indicates a well mixed profile up to the boundary layer top. The two-scale approach can approximately predict this observation; in contrast the local scheme fails. We find that the magnitude of the predicted wind speeds for both mixing schemes agrees well with the Lidar mean wind fields for the time period 1100 - 1200 LST and 1200 - 1300 LST. The two-scale approach leads to a slightly higher wind speed at the first model level. The difference between the two schemes at the first model level (20 m) is $\sim 0.2$ m/s.

There is no significant difference between the two-scale and local mixing
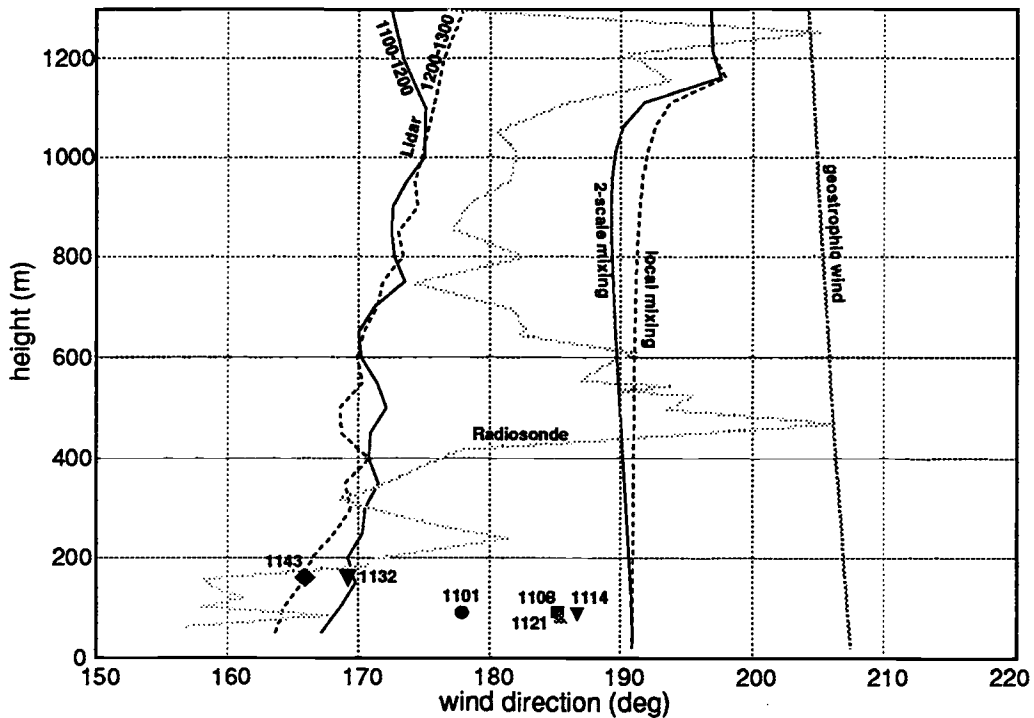
Figure 4.10: Model-predicted and observed wind direction (deg) for 28 July 1989 at 1200 LST during FIFE: individual symbols represent aircraft data.

scheme for the predicted wind directions (Fig. 4.10). The general direction for both the two-scale and local scheme is approximately 20 degree off clockwise from the Lidar observed profile. The wind direction predicted by the model is sensitive to the geostrophic wind direction which is prescribed in the model.

The profiles of wind speed and direction for 28 July 1989 from 1100 to 1700 LST show that the two-scale approach leads to well mixed profiles throughout most of the day where the local scheme predicts significant shear (Fig 4.11). The wind speed profiles at 1700 LST show shear for both schemes. The boundary layer grows into a layer of higher momentum and is therefore in transition. Also, turbulent mixing decreases in the late afternoon due to decreasing surface heating. The predicted direction of the wind vectors in the boundary layer are quasi-constant with height for both schemes (Fig 4.11).

There is significant scatter in the aircraft stress values (Fig 4.12). The data points for the aircraft legs starting at 1101 and 1132 LST are in good agreement
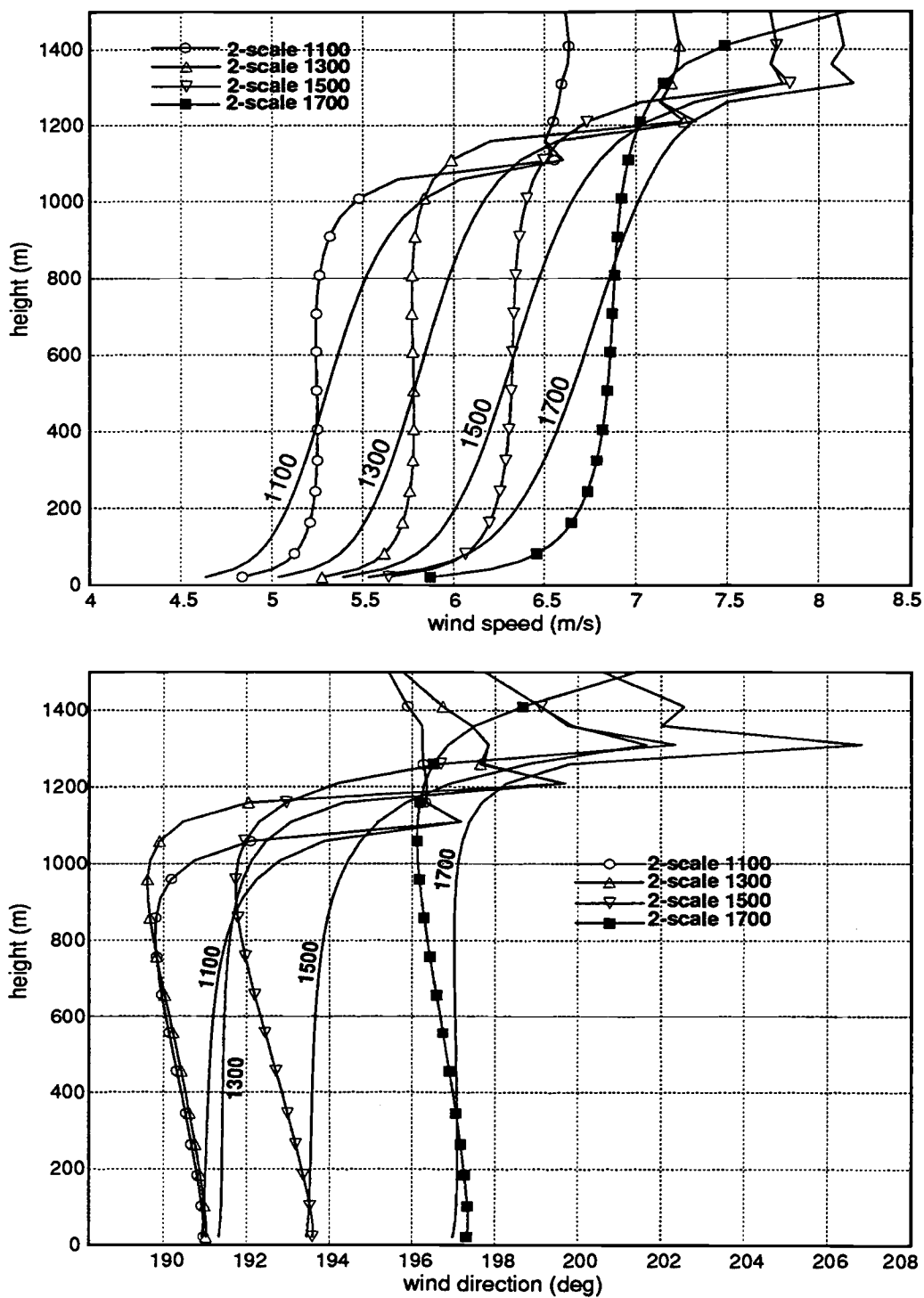
Figure 4.11: Model-predicted wind speed (m/s, top figure) and wind direction (deg, bottom figure) for 28 July 1989 during FIFE: Two-scale approach (solid lines with symbols) and local scheme (solid lines).
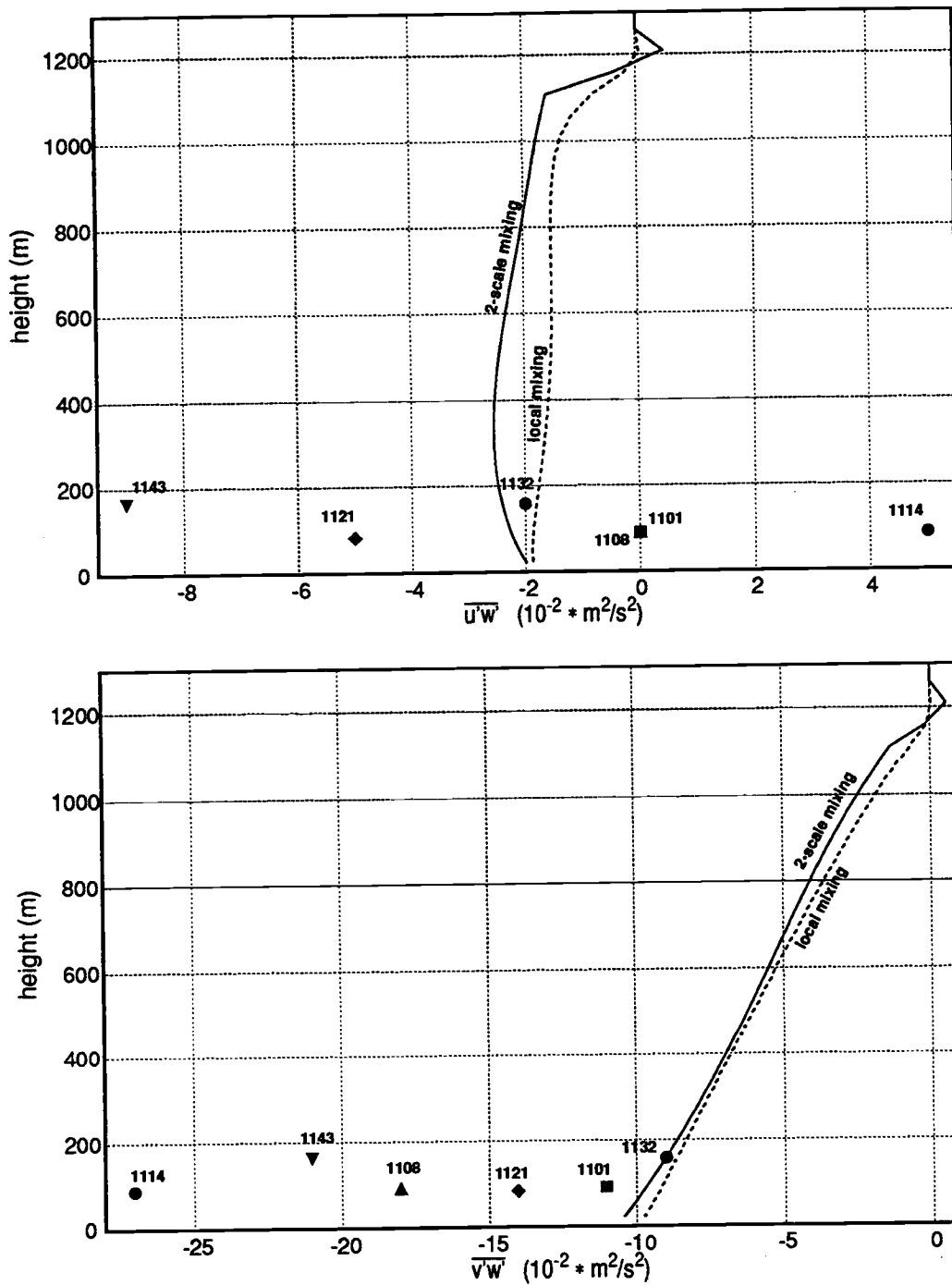
Figure 4.12: The components of the stress profile (m²/s²) for 28 July 1989 at 1200 LST during FIFE. Top figure, $\overline{u'w'}$; bottom figure, $\overline{v'w'}$. The aircraft flux values are indicated by the corresponding start time of the flight leg (LST).

Table 4.3: Predicted surface stress $u_*^2$ (m$^2$/s$^2$) and Obukhov length $L$ (m): A comparison between the prediction of the two-scale approach with $S_m = 1.4$ for 3 August, $S_m = 0.8$ for 28 July 1989, and a local mixing scheme.

| Day | $L$ (m) | | $-u_*^2$ ($10^{-2}\cdot$ m$^2$/s$^2$) | |
|---|---|---|---|---|
| | 2-scale | local | 2-scale | local |
| 3 August 1989, 1300 LST | $-106.51$ | $-93.05$ | 30.23 | 27.37 |
| 28 July 1989, 1200 LST | $-9.92$ | $-8.40$ | 10.6 | 9.90 |

with the corresponding model stress value at that level. This agreement is not a confirmation for the quality of the predicted stress profiles because of the uncertainties in the stress data obtained from aircraft measurements. The predicted surface stress values are listed in Table 4.3. The surface stress is increased by $\sim 9\%$ due to the nonlocal mixing of momentum.

In summary, the data comparisons show that the proposed two-scale mixing scheme improves the prediction of the momentum field in the boundary layer under windy conditions and it appears that the proposed nonlocal flux is appropriate. The difference between the first model layer velocities calculated from the two schemes has implications for the surface fluxes which are commonly parameterized in terms of the mean variables at the lowest model level. The two-scale approach leads to increased surface stress.

The comparisons in this study represent only cases of weak baroclinicity. The effects of stronger geostrophic shear on the model performance and $S_m$ will be investigated in the next section where we use sensitivity tests to evaluate the two-scale approach under several different atmospheric conditions.

## 4.5 Sensitivity Tests

We use 3 August 1989 as a background case to test the proposed mixing scheme for different values for the coefficient $S_m$ while keeping other external con-

ditions fixed. Fig. 4.13 shows the effect of $S_m$ on the wind speed and direction profile. Increasing $S_m$ leads to increased mixing of momentum resulting in more efficient downward transport of momentum. As the value of $S_m$ is increased beyond about 1.5, an unrealistic maximum develops in the wind profile. The "source" of the momentum maximum is related to the overprediction of the nonlocal flux. As $S_m$ decreases below 1.0 the profiles become less well mixed. The optimum value seems to be about 1.4 for the 3 August case.

As an alternative to the proposed parameterization of the nonlocal mixing, the value of the local eddy diffusivity $K_m$ could be increased, hoping that increased turbulent mixing would lead to better mixed momentum profiles. This approach requires that we ignore the inconsistency of using a purely local scheme to account for the nonlocal flux. Nevertheless, increasing $K$ by an factor of 10 leads to more well mixed profiles but at the same time numerical constraints make this approach unpractical. Also, it can be shown that a local mixing formulation can never lead to completely well mixed momentum. The momentum flux is written as $\overline{w'u'} = K_m \partial u / \partial z$ with $K_m$ described in (4.22). Assuming a well mixed momentum profile ($\partial u / \partial z \approx 0$) would imply zero stress, which contradicts the requirement that a well mixed momentum profile implies a linear flux profile under barotropic conditions. The prediction of shear in the mean boundary layer winds is inherent with this formulation.

We now examine the sensitivity to $S_m$ for baroclinic conditions. The problem is to find a general dependence of $S_m$ on baroclinicity. In a general sense we could expect the coefficient to be some function of $\partial u_g / \partial z$, $\partial v_g / \partial z$, $h$ and $w_s$ such as $(h/w_s)(|\partial \vec{u}_g / \partial z|)$. This nondimensional coefficient represents the product of the large eddy mixing time scale and the baroclinicity. The general dependence of the wind speed and direction profile on baroclinicity is not well known. The two days in FIFE were characterized by weak baroclinicity *and* well mixed boundary layers. From observations we do not know if momentum is well mixed under strong baroclinicity.
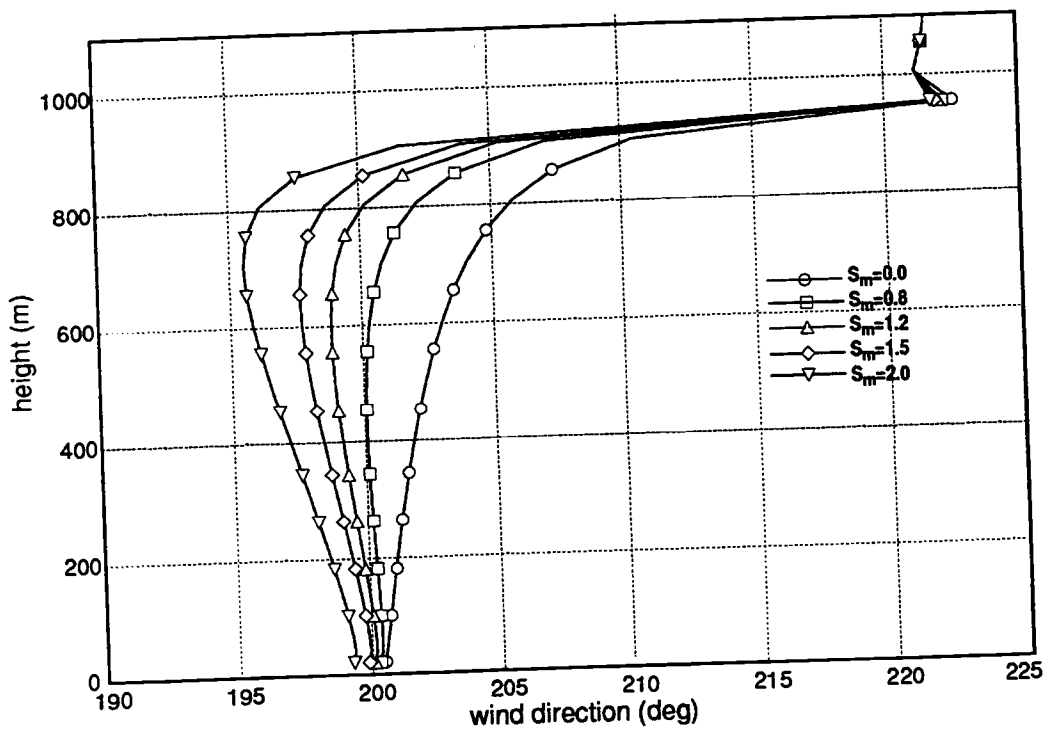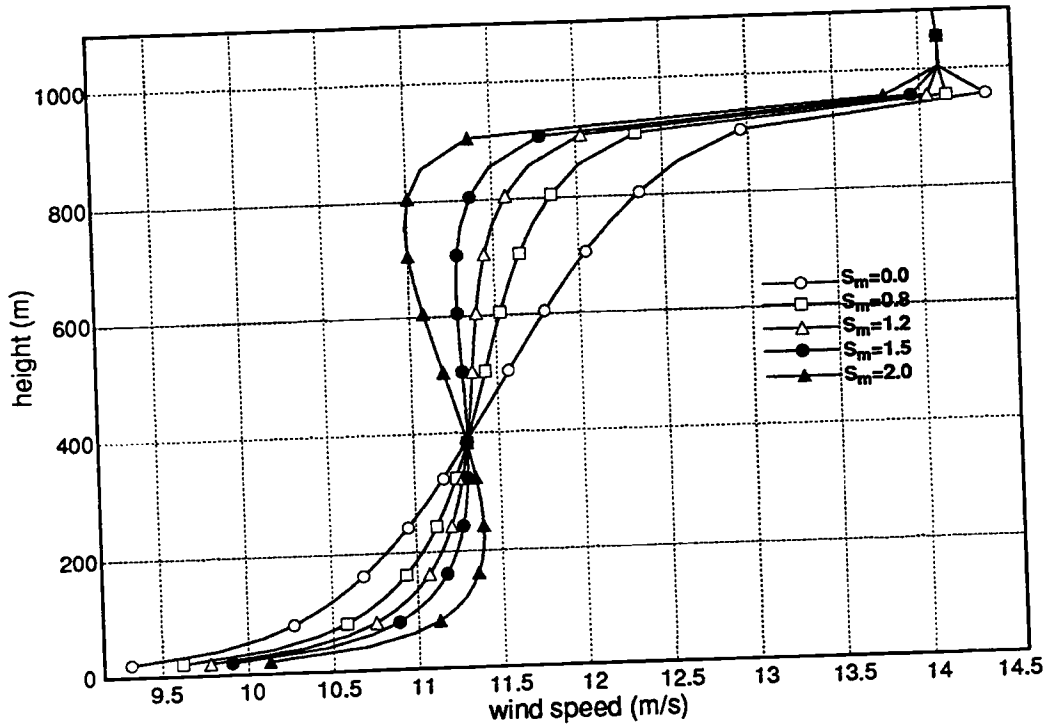
Figure 4.13: Sensitivity of the 2-scale approach on $S_m$ for August 1989 at 1300 LST: model-predicted wind speed (m/s, top figure), and wind direction (deg, bottom figure).
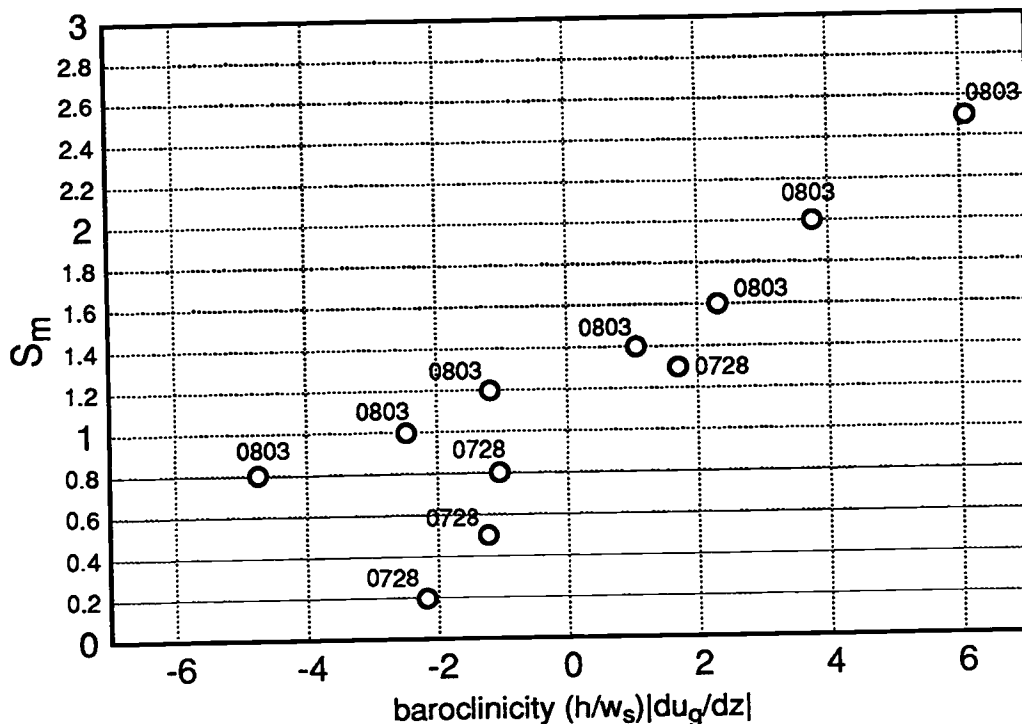
Figure 4.14: "Optimum" $S_m$ for producing well mixed momentum. Sensitivity of $S_m$ on baroclinicity factor with positive values corresponding to veering, and negative values corresponding to backing of the geostrophic wind. Each data point is labelled according to the day of the simulation. $du_g/dz$ is perpendicular to the geostrophic wind at the surface.

For instructional purposes, we examine the variation of $S_m$ under various degrees of baroclinicity as a function of the nondimensional coefficient $(h/w_s)$ $(|\partial \vec{u}_g/\partial z|)$. To illustrate the dependence of $S_m$ on baroclinicity, we choose $S_m$ such that the model predicts a well-mixed boundary layer. We find that the predicted wind speed profiles are sensitive to baroclinicity. A veering of the geostrophic wind requires an increase of $S_m$ in order to achieve a well mixed profile, and a corresponding decrease of $S_m$ for the backing case. We can interpret this sensitivity as the influence of the geostrophic shear on the boundary layer winds and the turbulent mixing. That we have to reduce $S_m$ in the case of a backing geostrophic wind is related to the fact that the geostrophic shear "counteracts" the veering of the wind vector in the boundary layer due to the frictional effect (the traditional Ekman layer profile). Therefore, the strength of the nonlocal mixing term needs not be as strong

in order to achieve the well mixed profile. The opposite is true for the veering of the geostrophic wind where well mixed conditions require an increased value of $S_m$. This case is equivalent to an increase of the mixing intensity.

We show the dependence of the required $S_m$ on geostrophic shear $(h/w_s)$ $(|\partial \vec{u}_g/\partial z|)$ at 1400 LST in Fig. 4.14. We show results using 3 August and 28 July as case studies where we specify different degrees of baroclinicity. We do not include the temperature advection associated with the thermal wind. We find that the choice of $S_m$ is not a simple function of baroclinicity. Unfortunately, it does not seem not possible to isolate a functional dependence of $S_m$ on baroclinicity from other parameters in the model.

In summary, the sensitivity tests indicate that relationship between the non-local mixing coefficient $S_m$ and the wind field under baroclinic conditions is complicated. The lack of observational evidence prevents a generalization of the proposed two-scale approach including the effect of baroclinicity on the mixing of momentum. Furthermore, the results perhaps indicate that a simple mixing formulation cannot represent the mixing of momentum under different atmospheric conditions. In particular, the proposed height dependence of the large eddy flux and its direction needs to be investigated. It seems that turbulent mixing of a vector is not as simple as we have assumed it in our two-scale approach. This can also be considered from another point of view. The parameterization of the large eddy stress followed closely the formulation for the large eddy heat flux which was derived from LES (Large Eddy Simulations; Holtslag and Moeng, 1991). They analyzed the budget equation for the heat flux in a convective boundary layer and showed that the heat flux can be expressed in terms of the local mean-gradient production term and a nonlocal contribution due to the turbulent transport term. Holtslag and Boville (1992) used this result and formulated the two-scale approach for heat described in Chapter 3. We therefore implicitly assume that the dominant terms in the budget equation for momentum (4.16) are the production of momentum flux by the mean shear and the turbulent transport term which lead to our proposed formulation for the large

eddy momentum flux (4.19). This implicit assumption might be not correct since for example pressure fluctuations are important for the momentum flux. So our formulation of the nonlocal flux (4.19) perhaps should be generalized by accounting for additional important terms in the budget equation for momentum (4.16) and which would in turn affect the height dependence of the large eddy momentum flux. Such an analysis might also explain why $S_m$ is not a simple function of baroclinicity. This would suggest the use of LES data.

# Chapter 5

# Conclusions

The two-scale mixing formulation for momentum was implemented to account for the momentum transport by large eddies in the simplest possible way. This makes the momentum transport scheme more consistent with existing formulations of heat and moisture transport. From the data comparisons we concluded that the two scale approach is able to better predict the observed well mixed mean structure of the momentum field under windy conditions. A local mixing scheme fails to predict the observed well mixed conditions. Unfortunately the "best" value of $S_m$ in the proposed two-scale approach depends on baroclinicity in a way that cannot be adequately determined with existing data. Quantitative data comparisons are difficult to make because of the uncertainties in the specified geostrophic wind and the omission of advection. Incorporating our 1-D model in a 3-D model would circumvent these problems.

The Lidar wind profiles are averaged in time and space and are therefore considered superior to radiosonde soundings and aircraft data, which have sampling problems. We concentrated our data comparison on two days in FIFE, since the Lidar data set is the only data set with reliable mean wind data. The two days in FIFE represent a mostly shear-driven (03 August) and a buoyancy-driven (28 July) boundary layer and both days were characterized by weakly baroclinic conditions. We showed that the scaling of the nonlocal momentum flux (4.19) appears to be appropriate for both flow regimes. A comparison of our approach with data obtained from other field programs would be inconclusive because there are typically no time-

and volume averaged mean momentum fields available.

The two-scale approach leads to increased surface stress due to the more effective downward transport of momentum. This finding is consistent with the direct numerical simulation of large eddies (Etling and Brown, 1993) which show the enhancement of the turbulent momentum flux by large eddies. This aspect may be important for operational or global models where the momentum transfer parameterizations typically do not account for the effect of large eddy mixing.

We cannot recommend a general functional dependence for $S_m$ based on the two days in FIFE. We showed that $S_m$ in (4.19) is not exclusively dependent on baroclinicity which is reflected by Fig. 4.14. But the data comparisons show some consistency based on the sensitivity tests for different baroclinic conditions: that is, for a backing of the geostrophic wind the value of $S_m$ has to be chosen smaller compared to a veering case. 28 July ($S_m = 0.8$) is characterized by a backing, and 3 August 1989 ($S_m = 1.4$) by a veering of the geostrophic wind.

The sensitivity tests indicated that mixing of a vector (momentum) is not simple. The height dependence of (4.19) is perhaps oversimplified and the implicit assumptions behind (4.19) are probably not always valid under different atmospheric conditions although (4.19) is appropriate in our data comparison. LES might be helpful to obtain a more general form for (4.19) but the lack of reliable observational data especially for strong baroclinic conditions perhaps limit the chance to obtain a simple generalization for (4.19).

The wind field of a baroclinic boundary layer should receive more attention. For example, the predictions of the wind field in the ECMWF model are generally poor under strong baroclinic conditions (Hollingsworth, personal communication). Obviously, there is need for a better understanding of the physical processes in a baroclinic boundary layer and for an improved momentum transfer parameterization under baroclinic conditions.

# BIBLIOGRAPHY

[1] Arya, S.P.S. and J.C. Wyngaard, 1975: Effect of baroclinicity on wind profiles and the geostrophic drag law for the convective planetary boundary layer. *J. Atmos. Sci.,***32**, 767–778.

[2] Beljaars, A.C.M, 1991: Numerical schemes for paramterizations. In *Numerical methods in atmospheric models, Volume II,* Reading, U.K., 9 – 13 September 1991. European Centre for Medium-Range Weather Forecasts.

[3] Bergström, H. and U. Högström, 1989: Turbulent exchange above a Pine forest II: Organized structures. *Bound.-Layer Meteor.,* **49**, 231–263.

[4] Brost, R. A., D. H. Lenschow and J. C. Wyngaard, 1982: Marine stratocumulus layers. Part I: Mean conditions. *J. Atmos. Sci.,* **39**, 800–817.

[5] Brost, R.A. and J.C. Wyngaard. 1978: A model study of the stably stratified planetary boundary layer. *J. Atmos. Sci.,* **35**, 1427–1440.

[6] Brown, R. A., 1982: On two-layer models and the similarity functions for the PBL. *Bound.-Layer Meteor.,* **24**, 451–463.

[7] Brown, R. A. and P. Mourad, 1990: A model for K-theory in a multi-scale large eddy environment. In *Preprints from the 9th Symposium on Turbulence and Diffusion,* Roskilde, Denmark, 30 April – 3 May 1990. American Meteorological Society.

[8] Deardorff, J. W., 1972: Theoretical expression for the countergradient vertical heat flux. *J. Geophys. Res.,* **77**, 5900–5904.

[9] Desjardins, R. L., R. L. Hart, J. I. MacPherson, P. H. Schuepp, and S. B. Verma, 1992: Aircraft- and tower-based fluxes of carbon dioxide, latent, and sensible heat. *J. Geophys. Res.,* **97**, 18,477–18,485.

[10] Ek, M. and L. Mahrt, 1991: A user's guide to osu1dpbl version 1.0.3: A one-dimensional planetary boundary layer model with interactive soil layers and

plant canopy. Technical report, Oceanic and Atmospheric Sciences, Oregon State University, Corvallis, OR 97331.

[11] Eloranta, E. W. and D. K. Forrest, 1992: Volume-imaging lidar observations of the convective structure surrounding the flight path of a flux-measuring aircraft. *J. Geophys. Res.*, **97**, 18,383–18,393.

[12] Etling, D. and R. A. Brown, 1993: Roll vorticies in the planetary boundary layer: a review. *Bound.-Layer Meteor.*, **65**, 215–248.

[13] Garratt, J. R., 1992: *The atmospheric boundary layer.* Cambridge University Press, 316 pp.

[14] Grossman, Robert L., 1992: Sampling errors in the vertical fluxes of potential temperature and moisture measured by aircraft during FIFE. *J. Geophys. Res.*, **97**, 18,439–18,443.

[15] Högström, Ulf, 1990: Analysis of turbulence structure in the surface Layer with a modified similarity formulation for near neutral conditions. *J. Atmos. Sci.*, **47**, 1949–1972.

[16] Højstrup, Jørgen, 1982: Velocity spectra in the unstable planetary boundary layer. *J. Atmos. Sci.*, **39**, 2239–2248.

[17] Holtslag, A. A. M. and B. A. Boville, 1993: Local versus nonlocal boundary layer diffusion in a global climate model. *J. Clim.*, **6**, 1825–1842.

[18] Holtslag, A. A. M. and C.-H. Moeng, 1991: Eddy diffusivity and countergradient transport in the convective atmospheric boundary layer. *J. Atmos. Sci.*, **48**, 1690–1698.

[19] Kelly, R. D., 1984: Horizontal roll and boundary-layer interrelationships observed over lake Michigan. *J. Atmos. Sci.*, **41**, 1816–1826.

[20] Lapidus, Leon and George F. Pinder, 1982: *Numerical Solution of partial differential Equations in Science and Engineering.* Wiley-Interscience, 677 pp.

[21] LeMone, M. A., 1976: Modulation of turbulence energy by longitudinal rolls in an unstable planetary boundary layer. *J. Atmos. Sci.*, **33**, 1308–1320.

[22] MacPherson, J. I., R. L. Grossman, R. D. Kelly, 1992: Intercomparison results for FIFE flux aircraft. *J. Geophys. Res.*, **97**, 18,499–18,514.

[23] Mahrt, L, 1991a: Eddy asymmetry in the sheared heated boundary layer. *J. Atmos. Sci.*, **48**, 472–492.

[24] Mahrt, L. and Wayne Gibson, 1992: Flux decomposition into coherent structures. *Bound.-Layer Meteor.*, **60**, 143–168.

[25] Pielke, Roger A., 1984 *Mesoscale Meteorological Modeling.* Academic Press, 612 pp.

[26] Piironen, A. K. and E. W. Elorenta, 1993: Volume Imaging Lidar results from FIFE 89: Boundary layer winds, depths, and cloud coverages. Technical report, Department of Meteorology, University of Wisconsin-Madison.

[27] Priestley, C.H.B. and W.C. Swinbank, 1947: Vertical transport of heat by turbulence in the atmosphere. *Proc. R. Soc.*, **A189**, 543–561.

[28] Puhakka, T. and P. Saarikivi, 1986: Doppler radar observations of horizontal roll vortices in Finland. In *23rd Conference on Radar Meteorology and Conference on Cloud Physics*, pages JP194–JP197, Boston. American Meteorological Society.

[29] Schols, J. L. and E. W. Eloranta, 1992: Calculation of area-averaged vertical profiles of the horizontal wind velocity from volume-imaging lidar data. *J. Geophys. Res.*, **97**, 18,395–18,407.

[30] Sellers, P. J., F. G. Hall, G. Asrar, D.E. Strebel, and R. E. Murphy, 1988: The First ISLSCP Field Experiment (FIFE). *Bulletin of Amer. Meteor. Soc.*, **69**, 22–27.

[31] Sellers, P. J., F. G. Hall, G. Asrar, D.E. Strebel, and R. E. Murphy, 1992: An Overview of the First International Satellite Land Surface Climatology Project (ISLSCP) Field Experiment (FIFE). *J. Geophys. Res.*, **97**, 18,345–18,371.

[32] Shaw, R. H., K. T. Paw and X. J. Zhang and W. Gao, G. Den Hartog and H. H. Neumann, 1990 Retrieval of turbulent pressure fluctuations at the ground surface beneath a forest. *Bound.-Layer Meteor.*, **50**, 319–338.

[33] Strebel, D. E., J. A. Newcomer, J. B. Ormsby, F. G. Hall, and P. J. Sellers,

1990: The FIFE Information System. *IEEE Trans. Geosci. Remote Sens.*, **28**(4), 703–710.

[34] Stull, R. B., 1988: *An Introduction to Boundary Layer Meteorology.* Kluwer Academic, Norwell, MA, 666pp.

[35] Therry, G. and P. Lacarrìe, 1983: Improving the eddy kinetic energy model for planetary boundary layer description. *Bound.-Layer Meteorol.*, **25**, 63–88.

[36] Troen, I. and L. Mahrt, 1986: A simple model of the atmospheric boundary layer: Sensitivity to surface evaporation. *Bound.-Layer Meteorol.*, **37**, 129–148.

[37] Wyngaard, J. C. and R. A. Brost, 1984. Top-down and bottom-up diffusion of a scalar in the convective boundary layer. *J. Atmos. Sci.*, **41**, 102–112.

[38] Zilitinkevich, S. S., 1973: Shear convection. *Bound.-Layer Meteorol.*, **3**, 416–423.

# Appendix A

# Numerics

## A.1   Introduction

This section discusses the numerical aspects related to the incorporation of the two-scale approach for momentum mixing in the OSU boundary-layer model. We briefly introduce the numerical scheme that is used in the model.

Numerical limitations require that the time-tendency of a variable due to different processes be computed separately. We can write the prognostic equation for a variable $\Psi$ in general form

$$\frac{\partial \Psi}{\partial t} = D_\Psi + P_\Psi \tag{A.23}$$

where $\Psi$ can be the wind components $u$ and $v$, temperature $T$ or specific humidity $q$. $D$ describes the dynamic time-tendency (including vertical advection) and $P$ the time-tendency of parameterized processes, here the vertical turbulent diffusion.

If we consider the prognostic equation for momentum, $D$ symbolizes the time-tendency due to the pressure gradient, Coriolis force and vertical advection. $P$ symbolizes the two-scale approach for the paramterization of turbulent diffusion. The nonlocal flux of momentum is posed as a forcing term in the diffusion equation. The turbulent diffusion part "$P_m$" of the prognostic equation is

$$\frac{\partial u}{\partial t} = \frac{\partial}{\partial z}\left(K_m \frac{\partial u}{\partial z}\right) + \frac{\partial F_L(z)}{\partial z} \tag{A.24}$$

where $\partial F_L/\partial z$ is the nonlocal flux divergence of momentum. Note, that $F_L$ (4.19) is not a function of $u$ which is the variable we solve for in (A.24). Alternatively, we

can apply the method of a gradient correction (see Chapter 2) writing the nonlocal flux of momentum in terms of the local eddy diffusivity $K_m$ (4.22):

$$\frac{\partial u}{\partial t} = \frac{\partial}{\partial z}\left(K_m\left(\frac{\partial u}{\partial z} + \gamma_m\right)\right) \tag{A.25}$$

with the gradient correction $\gamma_m$ derived from (4.19):

$$\gamma_m = S_m \frac{u_*(w_* + u_*)}{w_s k h} \tag{A.26}$$

We apply the explicit leap-frog technique for the time integration because of its computational efficiency. It is applied to the time-tendency due to dynamic forcing but cannot be used for the parameterized sub-grid process, here turbulent diffusion of momentum. The explicit leapfrog scheme is unconditionally unstable for these processes (described by a parabolic partial differential equation). We compute the turbulent diffusion by an implicit Crank-Nicholson scheme in a finite element domain (for more details see Ek and Mahrt, 1991).

In our current finite difference approximation, the time-tendency has a truncation error of order $\Delta t^2$ (for both the implicit and explicit formulation we use centered time differencing) and a spatial truncation error of the order $\Delta z^2$.

## A.2  Time Truncation Error and the Importance of Integration Order

The current integration order can be classified as a "process splitting technique" (Beljaars, 1991). We calculate the time-tendency of momentum due to turbulent diffusion and the dynamic forcing separately based on the wind field at time level $n - 1$. The two time tendencies update the new field to the time level $n + 1$. This splitting into dynamic and subgrid processes separates the governing equation into two time-dependent equations. A time filter is necessary to prevent the different processes from decoupling.

Two aspects need to be addressed. First, how do the truncation errors in time and space due to finite difference approximations of the governing equation

influence the physical force balance? Second, how does the order of integration affect the model results? The aspect of the time truncation error previously appeared to be a problem in the boundary layer scheme of the ECMWF model (Beljaars, 1991). It was found that the surface stress had systematically lower values than expected from the first model level wind field. The error was related to the order of integration.

The order of integration is important since different timescales are involved in the prognostic equation (in a convective boundary layer, the turbulent time scale is on the order of 10 minutes and the mesoscale/synoptic scale is on the order of 2 hours). Typically, numerical schemes in simple boundary layer models do not account for the different timescales present in the prognostic equation (A.23). The time step in these models essentially imposes a timescale. Consequently, we have to ensure a physically reasonable force balance when we use long time steps.

From a modeling point of view, the turbulent diffusion scheme brings the wind field from time level $n-1$ into an equilibrium at level $n+1$ without accounting for the influence of the dynamic forcing in the case of the "process splitting method". The resulting time-tendency due to the diffusion process and the dynamic terms can lead to a wrong equilibrium wind field especially if long time steps (e.g. 600 sec. or greater) are used; the force balance could be erroneous. This integration order is currently applied in our model and was used in the ECMWF boundary layer scheme.

Beljaars (1991) proposed an order of integration called the "method of fractional steps" and suggested that physical processes should be ordered along their characteristic timescale. For the case of momentum we would first compute the time-tendency due to the "slow" dynamic terms (explicit time integration) and use this updated wind field for the fast diffusion process (implicit time integration). The eddy diffusivity is based on the variables at time level $n-1$. This method improved the performance of the ECMWF model (Beljaars, 1991).

We investigate one other numerical method using local composites (Lapidus
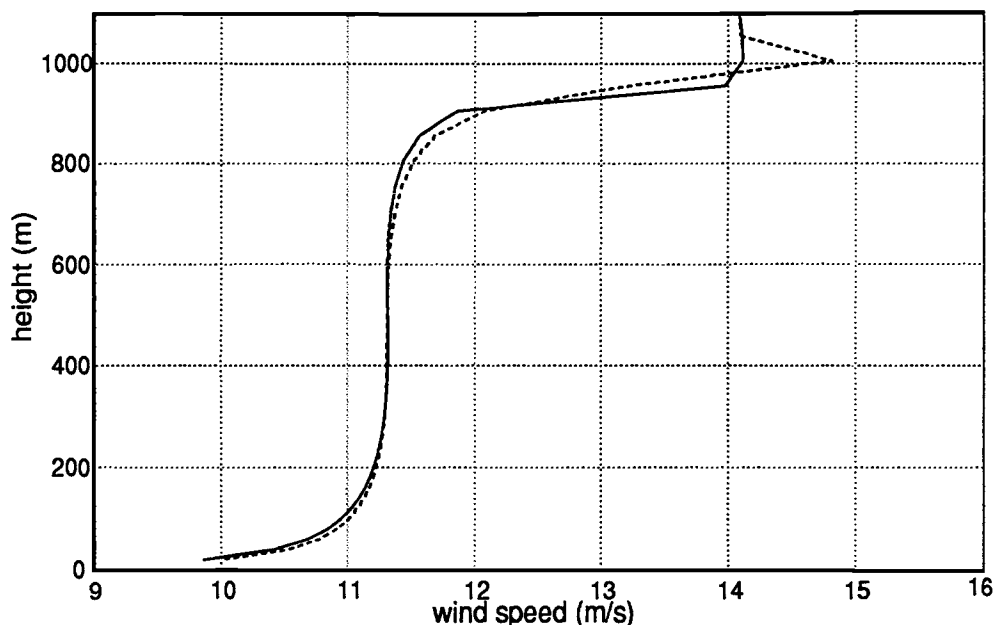
Figure A.1: Predicted wind speed (m/s) for 3 August 1989: The "forcing method" with $S_m = 1.4$ (solid line) versus the gradient correction method (dashed line) with $S_m = 1.8$ using $\Delta t = 60$ sec.

and Pinder, 1982) which reduces the time truncation error. Furthermore, this method has the advantage that it improves the numerical stability of the applied numerical scheme. The general idea is to split the time step into intervals and solve the turbulent diffusion equation with these sub-steps to integrate up to the time level $n + 1$. We test local composites for the "method of fractional steps".

Including the nonlocal flux of momentum as a gradient correction (see A.25) is comparable to the method of "fractional steps". Here, the wind field is updated by the gradient correction *before* the numerical solution of the diffusion equation. The method of fractional steps cannot be applied when we use the gradient correction to include the nonlocal flux of momentum because updating the wind field by the dynamic terms and by the nonlocal contribution before the diffusion equation is solved leads to an erroneous time-tendency of the wind field. We found an erroneous prediction of the wind speed.
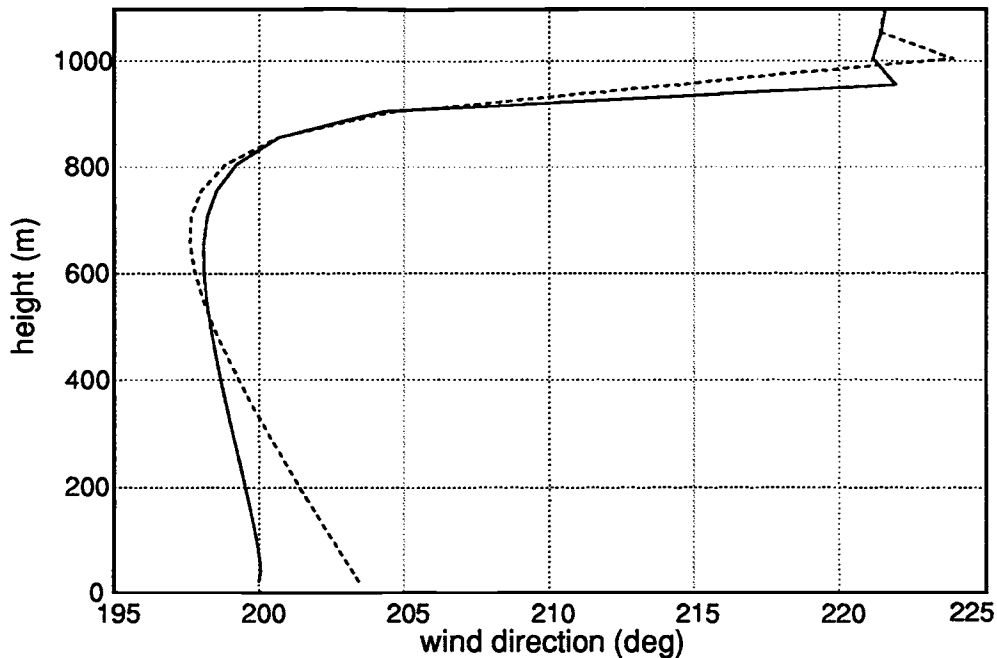
Figure A.2: Predicted wind direction (deg) for 3 August 1989: The "forcing method" with $S_m = 1.4$ (solid line) versus the gradient correction method (dashed line) with $S_m = 1.8$ using $\triangle t = 60$ sec.

## A.3 Numerical Tests

We test the different numerical methods using 3 August 1989 at 1300 LST during FIFE as a background case. We used a time step of 60 sec and a spatial resolution of 70 grid levels ($\triangle z = 20$ to 50 m) for data comparisons in Section 4.4. Typically, the time step is 600 sec or greater in operational large scale model runs with a coarse grid (e.g. $\triangle z = 100$ m). We first summarize the keywords and explain the corresponding computational procedure that is employed to predict the momentum field at time level $n + 1$ starting from level $n - 1$:

**"The reference profile"** This profile is predicted using $\triangle t = 60$ sec. We include the nonlocal flux of momentum as described with (A.24). We expect a small truncation error and the prediction is not sensitive to the integration order.

**"Process splitting"** We split the time-tendency equation (A.23) into two independent parts which are solved separately
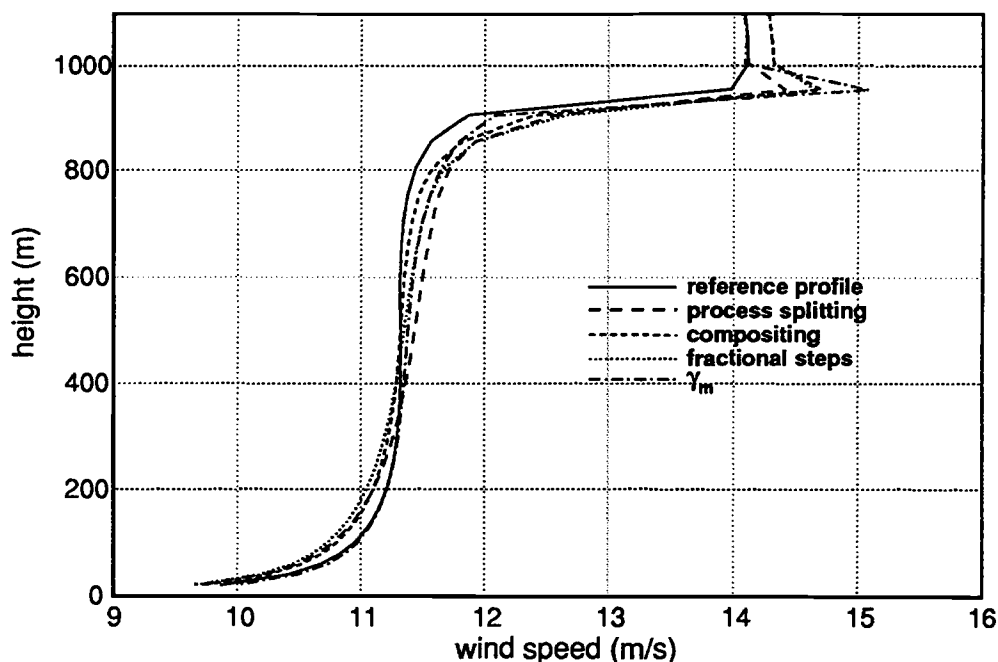
Figure A.3: Predicted wind speed (m/s) for 3 August 1989: $\Delta t = 600$ sec. The profiles (at 1300 LST) show the sensitivity of the predicted profiles on the choice of the integration order. The reference profile is obtained with $\Delta t = 60$ sec. All profiles are calculated on a high resolution grid. The gradient correction method ($\gamma_m$) uses $S_m = 1.8$, where the other schemes use $S_m = 1.4$. The "compositing method" is based on 3 even sub-time steps.

**"Fractional steps"** We update the dependent variable with the dynamic forcing, and solve the diffusion equation with the updated variable with the local eddy diffusivity $K$ based on time level $n - 1$.

**"Compositing"** The underlying integration order is the method of "fractional steps"; the time step for the diffusion part (A.24) is divided into even sub-time steps (the number of time intervals is indicated in the graphs). The final time-tendency is calculated by integrating the tendencies based on the sub-time steps up to level $n + 1$.

**"$\gamma_m$"** Indicates the method of the "gradient correction"

We first show the results for the fine resolution version of the model using different time steps. We do not show the plots for all the different computational procedures with $\Delta t = 60$ sec since the differences between the numerical tests are
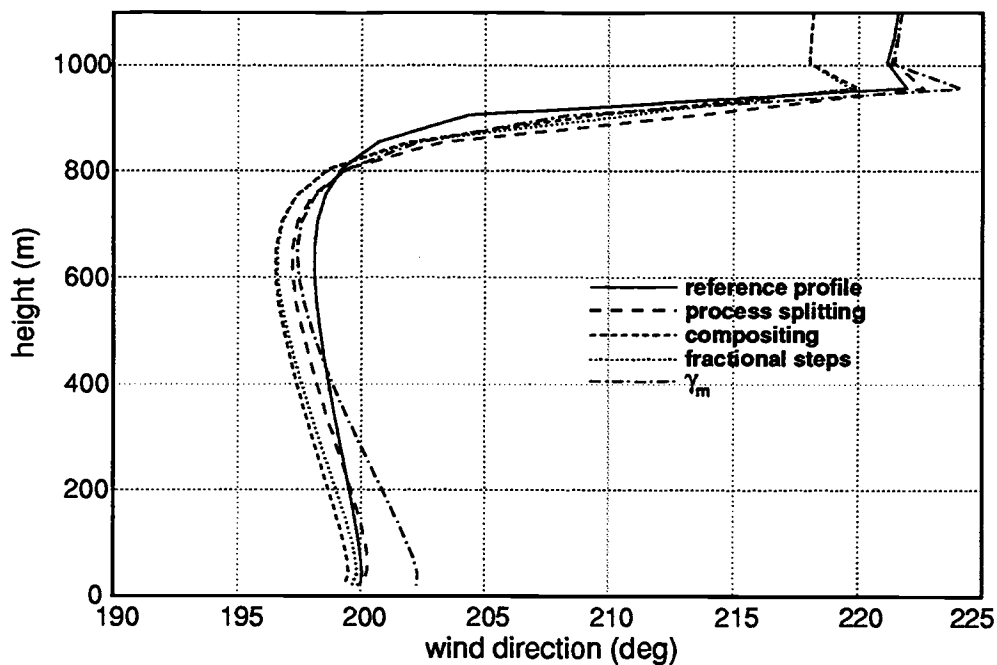
Figure A.4: Predicted wind direction (deg) for 3 August 1989: $\Delta t = 600$ sec. See the comments in Fig. A.3
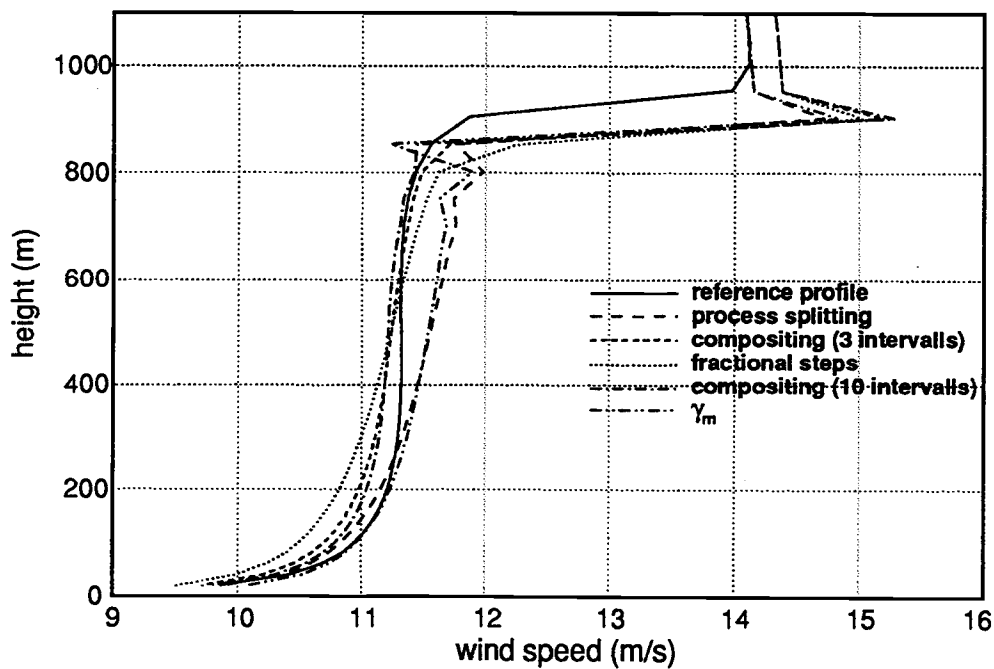


Figure A.5: Predicted wind speed (m/s) for 3 August 1989: $\Delta t = 1800$ sec. See the comments in Fig. A.3. We show the "compositing method" with 3 and 10 even sub-time steps.
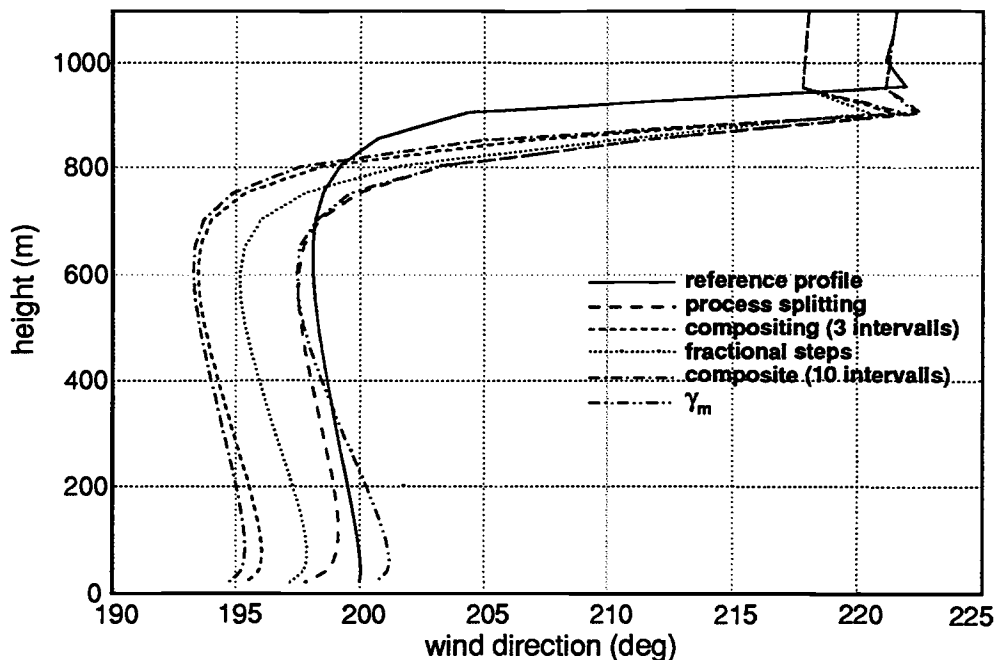
Figure A.6: Predicted wind direction (deg) for 3 August 1989: $\Delta t = 1800$ sec. See the comments in Fig. A.3. We show the "compositing method" with 3 and 10 even sub-time steps.

negligible indicating that the time and spatial truncation errors are small. Figure A.1 shows the wind speed predicted by the "forcing method" using $S_m = 1.4$ in comparison to the "gradient correction method" with $S_m = 1.8$ for $\Delta t = 60$ sec. The increase of $S_m$ is related to the different order of integration. We see that there is essentially no difference between the two wind speed profiles. The gradient correction method shows some noise near the boundary layer top presumably related to the order of integration. The difference in the wind direction (Fig. A.2) is related to the slightly higher wind speed in the lower part of the boundary layer.

Figure A.3 shows the wind speed profile using $\Delta t = 600$ sec. All methods predict weak shear in the wind profile which can be explained by the time truncation error since we test the numerical scheme on a high resolution grid. The "compositing method" can reduce the time truncation error considerably and is closest to the reference profile. The composite in Fig A.3 is based on three even sub-time steps. The difference between the method of "fractional steps" and the "process splitting" is small, and the gradient correction appears to be not as much affected by the

truncation error as these two methods. The wind directions are not significantly different for the applied methods (Fig. A.4).

The tests with $\triangle t = 1800$ sec show the increasing effect of the time truncation error (Figs. A.5 and A.6). The results near the boundary layer top for the gradient correction and the process splitting methods suggest that this time step with the fine spatial resolution becomes numerically unstable. The growing mode probably can be found in the explicit part of the numerical scheme, where the explicit approximation of the Coriolis force is numerically unstable (see e.g. Pielke, 1984). But there is no definite answer possible since the numerical modes are dependent on each other. Local composites can reduce the truncation error and the shear in the wind profile. Additionally, the scheme becomes numerically stable which can be seen in the predicted wind speed profile near the boundary layer top. In comparison to the reference profile, all numerical methods show shear in their corresponding wind speed profile.

We now check the numerical results when we use a coarser grid (25 levels with $\triangle z = 50$ to 100 m). Errors due to the spatial resolution can be important for these tests. Fig. A.7 shows the predicted wind speed with $\triangle t = 600$ sec. The differences in the predicted wind speeds and directions (Fig. A.8) which represent the applied methods are small. The fact that the profiles are well mixed for these tests could be explained by arguing that the spatial truncation error balances the time truncation error. The tests with $\triangle t = 1800$ sec show that the method of "process splitting" and "fractional steps" have significant shear (Fig. A.9). The method of local composites leads to a well mixed wind profile in the interior of the boundary layer, but wind speed decreases towards the boundary layer top which is perhaps related to the coarse spatial resolution. The method of a gradient correction works best in this test and agrees well with the reference profile; there is also good agreement between the predicted wind directions (Fig. A.10).
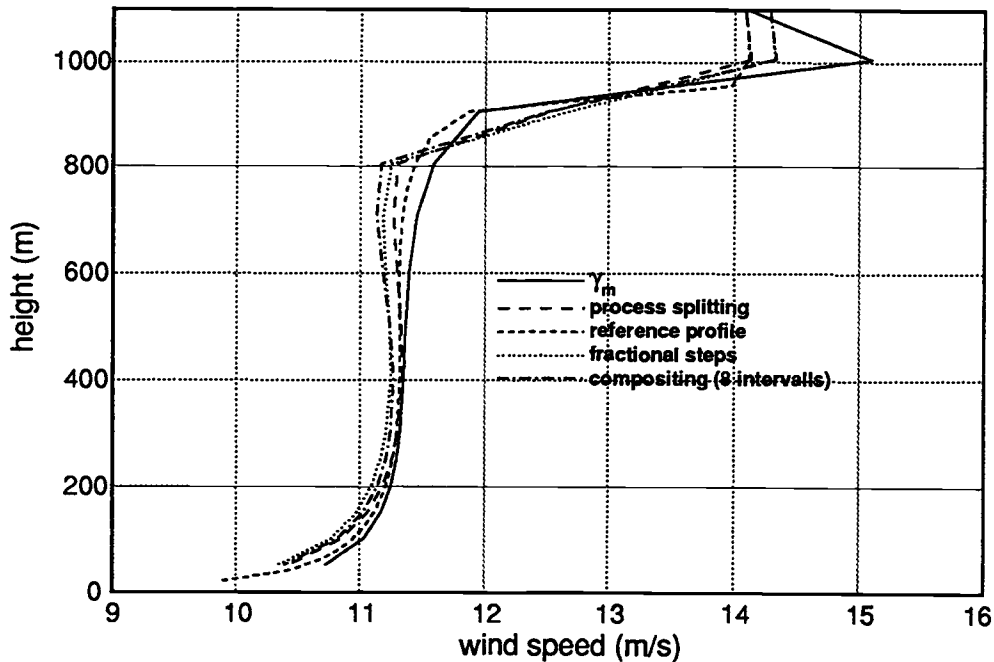
Figure A.7: Predicted wind speed (m/s) for 3 August 1989: $\Delta t = 600$ sec. The profiles (at 1300 LST) show the sensitivity of the predicted profiles on the choice of the intergration order. The reference profile is obtained with $\Delta t = 60$ sec. and on a high resolution grid. The other profiles are predicted on a coarse grid. The gradient correction method ($\gamma_m$) uses $S_m = 1.8$, where the other schemes use $S_m = 1.4$. We show the "compositing method" with 8 even sub-time steps.

## A.4 Conclusions

The tests show the numerical problems related to time truncation errors when we incorporate the two-scale approach for momentum in a numerical model. The complications we found in the previous section can be explained by the nature of the two-scale approach: the nonlocal flux is posed as an analytical function in $z$. Consequently, there is no additional truncation error in time and space due to finite difference approximations when we implement the nonlocal flux in the numerical scheme. The value for $S_m$ has been determined by sensitivity tests using a fine resolution model. Using a different time step changes the time-truncation error which leads e.g. to shear in the wind speed profile as seen in Fig. A.3. We conclude that $S_m$ should be also a function of the truncation error in addition to baroclinicity and stability. A gradient correction appears to be a robust method, especially for
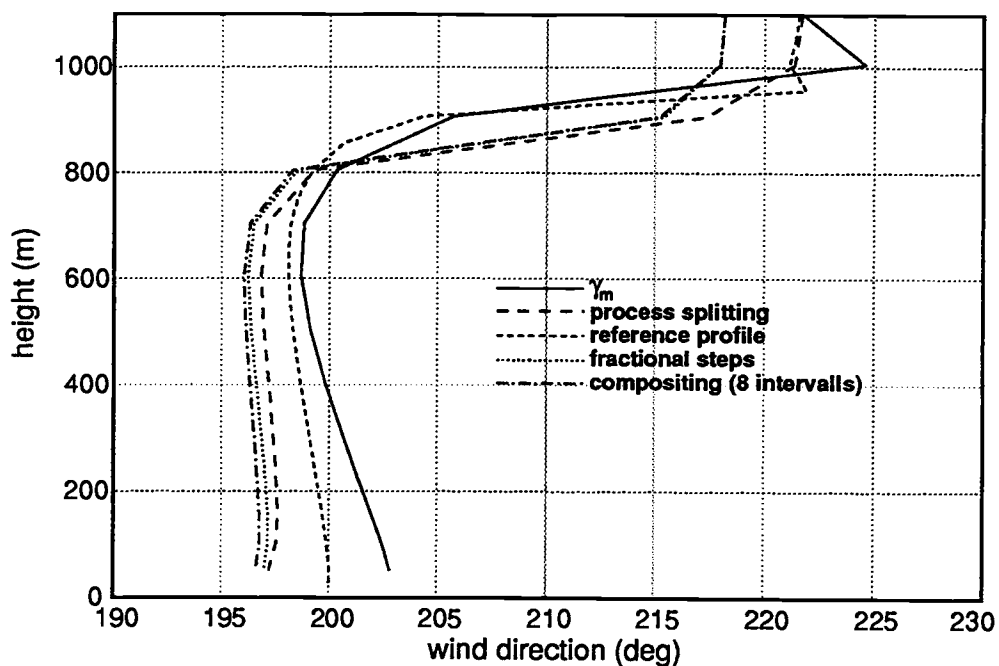
Figure A.8: Predicted wind direction (deg) for 3 August 1989: $\Delta t = 600$ sec. See the comments in Fig. A.7.
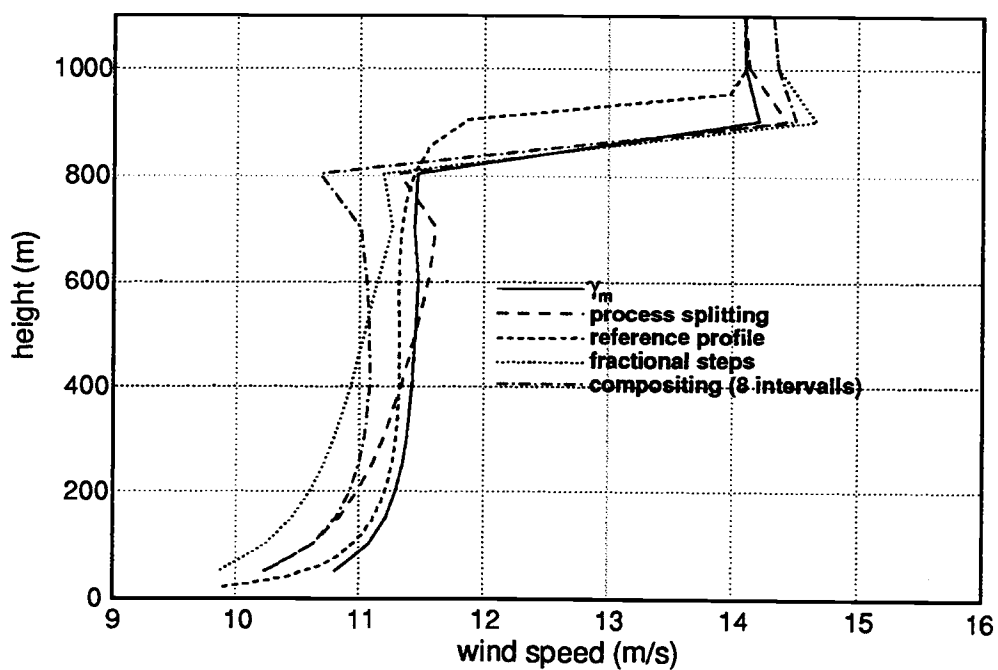


Figure A.9: Predicted wind speed (m/s) for 3 August 1989: $\Delta t = 1800$ sec. See the comments in Fig. A.7.
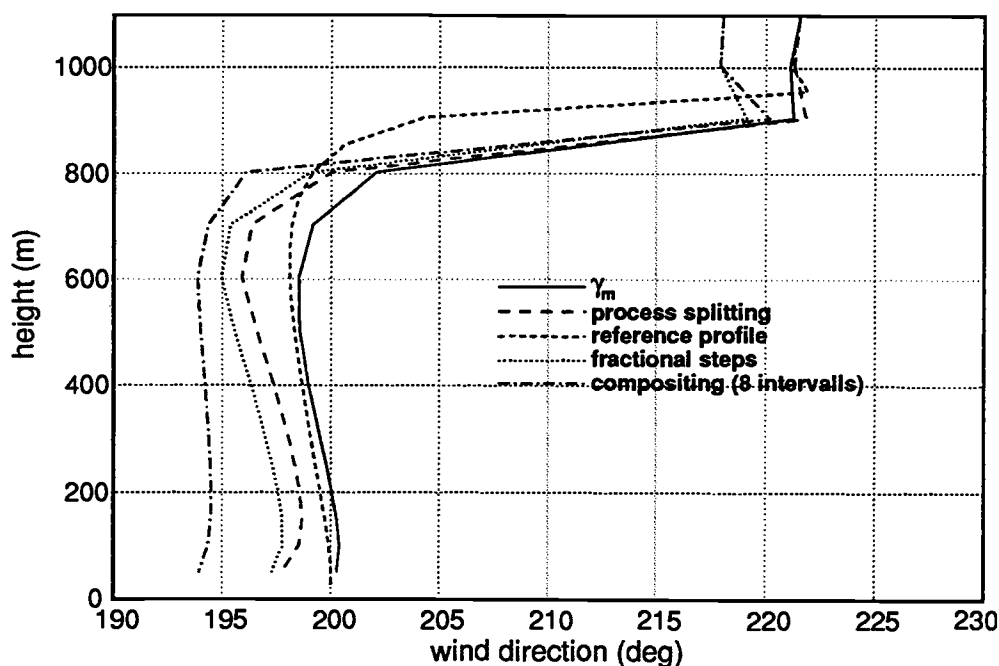
Figure A.10: Predicted wind direction (deg) for 3 August 1989: $\Delta t = 1800$ sec. See the comments in Fig. A.7.

the tests with a coarse spatial resolution and a long time step (Fig. A.10). But it is more consistent to introduce the nonlocal flux as a forcing term in the diffusion equation (A.24). That is, the wind field is subject to local and nonlocal turbulent diffusion at the same time. Local composites in connection with the method of "fractional steps" improve the results as we found for the fine grid model version. If the model is used in a "stand-alone" version, this method seems to be best. Also, this method is physically more appealing since we approximately account for the different time-scales involved in the prognostic equation. Furthermore, we increase the numerical stability of the model. When computation time is an important factor this method should be avoided. It might be beneficial to develop a new numerical scheme with a higher degree of accuracy. Since our two-scale approach appears to be sensitive to the time truncation error, an approximation of the time-tendency based on more time levels can improve the model performance. Computationally, we would have to store more variables at additional time steps which is a disadvantage.

# Appendix B

# Surface Flux Stations in FIFE

Table B.1 lists the surface flux stations that are available in FIS for the 28 July and 03 August.

| Day | Station Number |
|---|---|
| 28 July 1989 | 902, 904, 906, 908, 910, 912, 913, 916, 924, 926, 936, 944 |
| 03 August 1989 | 902, 908, 910, 912, 926, 938 |

Table B.1: A list of surface flux stations with available surface flux data for 28 July and 3 August 1989; see fig. 4.1 for the locations of the stations.

# Appendix C

# Modeling the 03 August and 28 July 1989 of FIFE

For comparison with the model, we area-average arithmetically the point measurements of the surface flux stations in the FIFE domain without weighting each station according to site aspect, slope and vegetation cover. The available stations are not randomly distributed over the FIFE site, which in turn bias the averaged flux values (see Fig. 4.1; the stations with available surface flux data for the two days we study are listed in Appendix B). Fluxes of sensible and latent heat from aircraft measurements are usually underestimated by 10% in FIFE 1989 due to sampling problems (Desjardins *et al.* 1992).

A comparison of the area averaged surface fluxes with fluxes measured using the Twin Otter aircraft shows significant variation (Figs. C.1 and C.2). To account for the height dependence of the fluxes we increase aircraft fluxes by 10%. The difference between aircraft fluxes and fluxes from surface stations seems to be not explained by the potential underestimation of the fluxes by the aircraft, rather it appears to be related to the variable cloud cover. The large fluxes observed by the surface flux stations around 1200 LST for 3 August seems to collaborate with this suggestion. The spatial variability for both days complicates a comparison of model results with observations.

We briefly discuss the prediction of boundary layer height $h$ and the surface fluxes in our data comparisons. There is a high degree of variability in the observed data which consequently makes comparisons with model results difficult.

On the 03 August, the predicted surface fluxes agree reasonably well from
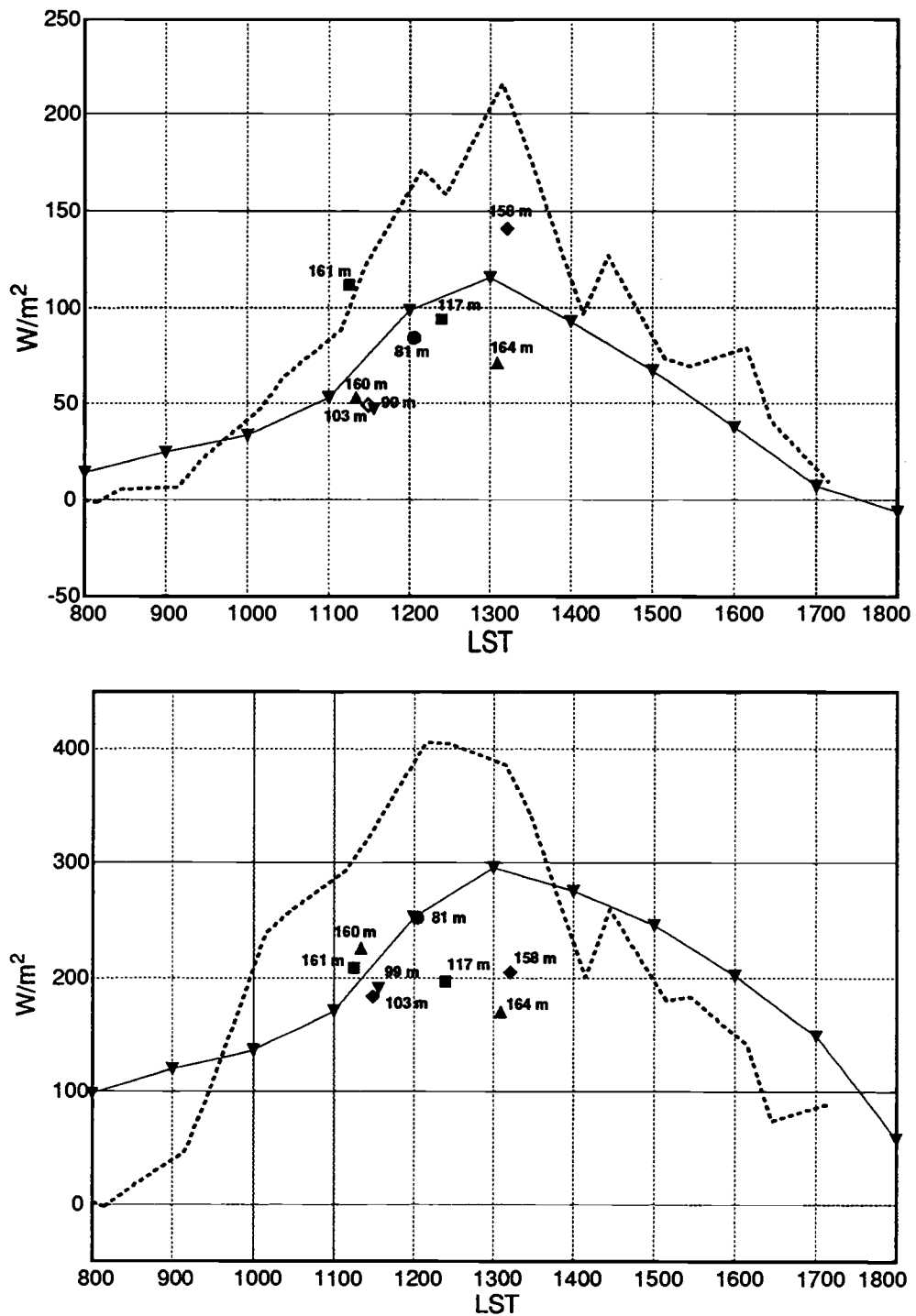
Figure C.1: Sensible heat flux (W/m$^2$, top figure) and latent heat flux (W/m$^2$, bottom figure) for 3 August 1989 during FIFE: surface observations (dashed), model predicted (solid) and aircraft data (symbols). The heights (m) near the symbols indicate aircraft height.
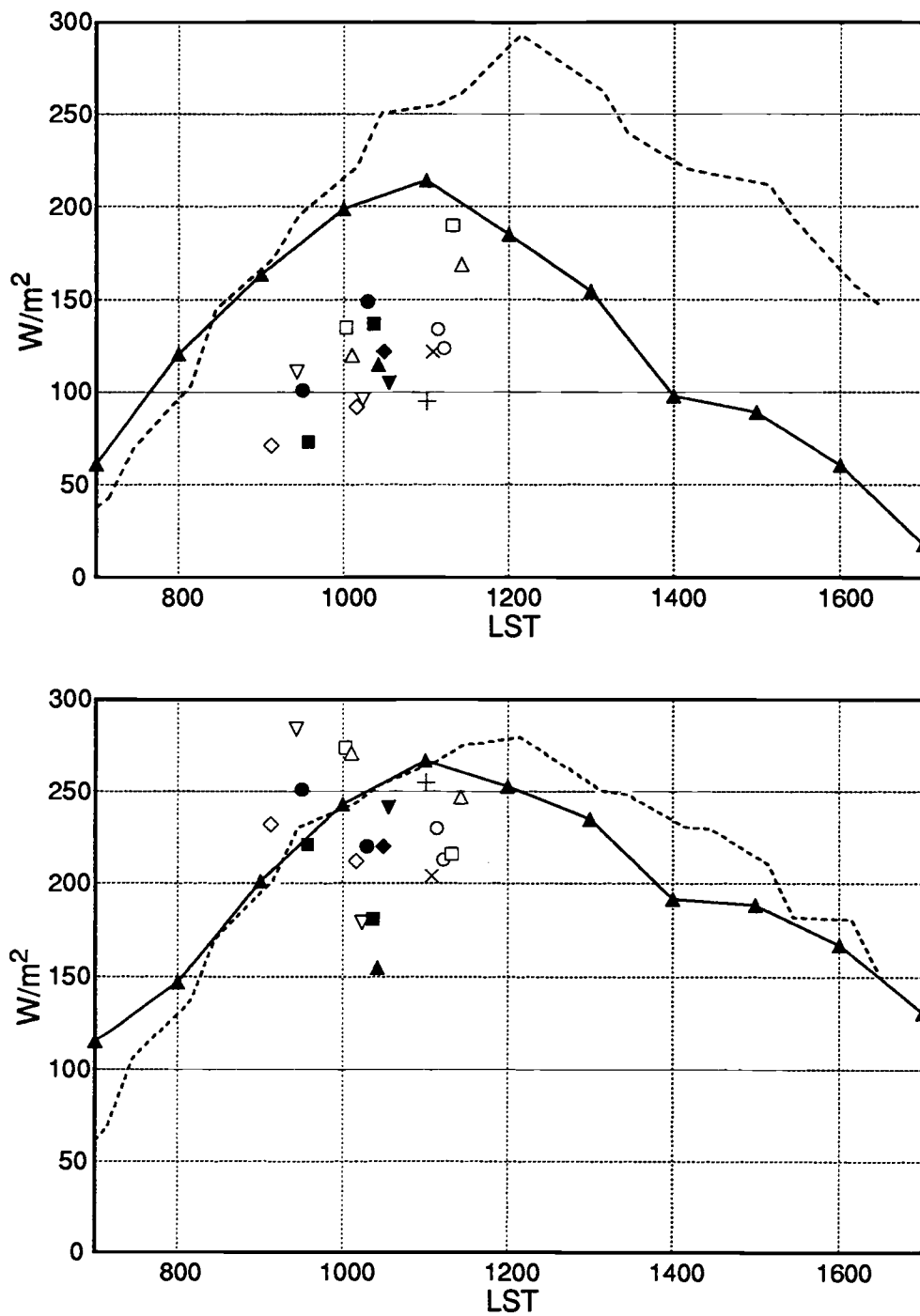
Figure C.2: Sensible heat flux (W/m², top figure) and latent heat flux (W/m², bottom figure) for 28 July 1989 during FIFE: surface observations (dashed), model predicted (solid) and aircraft data (symbols). The aircraft flux data corresponds to heights between 76 m and 164 m.

1400 LST on with the aircraft data supporting the predicted model fluxes. This coincides with the small fractional cloud cover observed by the Lidar (Fig. C.1). The predicted $h$ is initially to be too high (Fig. 4.2), however the definition of a mean boundary layer height obtained from Lidar data is ambiguous in the presence of clouds since we have to account for the cloud type (Stull, 1988) and the influence of clouds on the turbulent mixing in the boundary layer. The Lidar data set essentially defines the cloud base to be the boundary layer top. The cloud base is near 278 m with the corresponding $h$ of 323 m at 1138 LST, and the cloud top at 915 m (Piironen and Eloranta, 1993).

The results for 28 July show approximate agreement with the model for the area averaged surface fluxes and aircraft sensible heat flux and until 1000 LST when clouds start to evolve (Fig. 4.3). The model surface fluxes continue to agree with the aircraft fluxes through 1200 LST (Fig. C.2). The observed fluxes indicate that they seem to be not affected by Lidar-observed cloud cover. Presumably, the small sensible heat flux predicted by the model compared to the area-averaged fluxes can be explained by the reduced incoming solar radiation. The boundary layer height $h$ (Fig. 4.3) initially grows too deep compared to the observed mean boundary layer height. The relatively high initial surface heat flux predicted by the model compared to the area averaged fluxes leads to deeper growth of $h$. The predicted $h$ is in good agreement with the observed $h$ after $\sim$ 900 LST. The comparison of model surface fluxes with observed fluxes suggest that the prescribed cloud cover might be only representative for the Lidar domain and not for the whole $15 \times 15$ km$^2$ domain leading to the observed disagreements. Other potential sources of disagreement could be the overestimation of the cloud cover by Lidar, or the use of the simple plant-soil model (that is coupled with the boundary-layer mixing model which has no time-dependent canopy resistance.

Fig. C.3 shows the predicted potential temperature profile at 1300 LST in comparison with aircraft measurements for 3 August 1989 (no radiosonde sounding was available at this time). The model is roughly 1.5 K too cool if we assume that
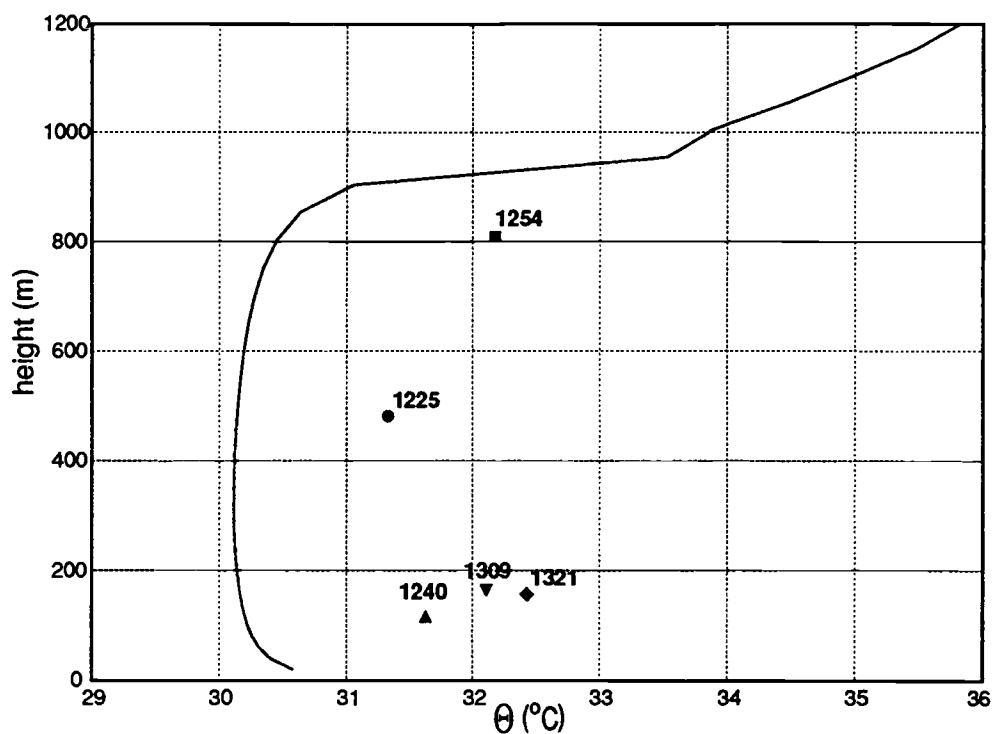
Figure C.3: Potential temperature profile (°C) for 3 August 1989 at 1300 LST during FIFE; symbols represent aircraft data.

the aircraft provides a reliable mean temperature field. The uncertainties caused by the variable cloud cover complicates a comparison with observational data. It is possible that warm air advection is also important.